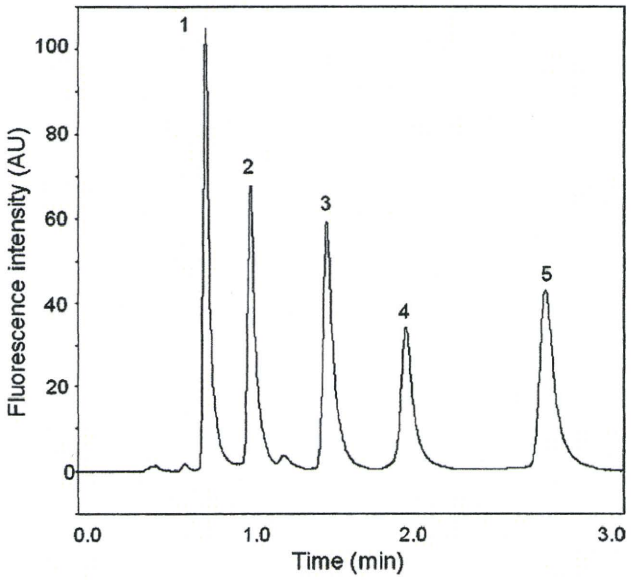

Fig. 2. Chromatogram of doxorubicin and its metabolites. The chromatographic conditions are described in Section 2. 1, doxorubicinol; 2, doxorubicin; 3, doxorubicinolone; 4, daunorubicin (internal standard); 5, doxorubicinone.

standard deviation (R.S.D.) of each peak was less than 0.13% ($n = 5$), for each analyte, at a concentration of 50 ng/mL. The conditions of separation of doxorubicin and its three metabolites were very simple in that the elution was isocratic, and the mobile phase consisted of only two different solvents, whereas some reported methods require three different solvents [7,8]. Fig. 3a is a chromatogram of a homogenate from untreated HeLa cells, and Fig. 3b is a chromatogram of an equivalent homogenate spiked with doxorubicin and its metabolites at a concentration of 500 ng/mL. No interfering peaks were observed, and doxorubicin, the three metabolites, and the internal standard separated well. These results show that the separation conditions were optimized with selectivity to each compound.

3.2. Detection limits and quantitation limits

Detection limits and quantitation limits of doxorubicin and its metabolites were determined based on the signal-to-noise approach, (S:N ratio, 3:1 for detection limits and 10:1 for quantitation limit) (Table 1). The quantitation limits of doxorubicin, doxorubicinol, doxorubicinolone, and doxorubicinone ranged between 11.7 and 24.5 pg/injection. The quantitation limit of 17.4 pg/injected doxorubicin (32.0 fmol/injected doxorubicin) was about 2 times lower than the limit ever reported using conventional HPLC [8], and more than 10 times lower than other reported values [7,9–11]. We suggest that the high resolution and sensitivity of UHPLC are responsible for this improvement.

Table 1
Detection limits and quantitation limits of doxorubicin and its metabolites.

Compound	Detection limit (pg/injection)	Quantitation limit (pg/injection)
Doxorubicin	5.2	17.4
Doxorubicinol	3.5	11.7
Doxorubicinolone	6.0	19.8
Doxorubicinon	7.4	24.5

The detection and quantitation limits of doxorubicin and its metabolites were determined based on signal-to-noise ratios (3:1 for detection limits, and 10:1 for quantitation limits).

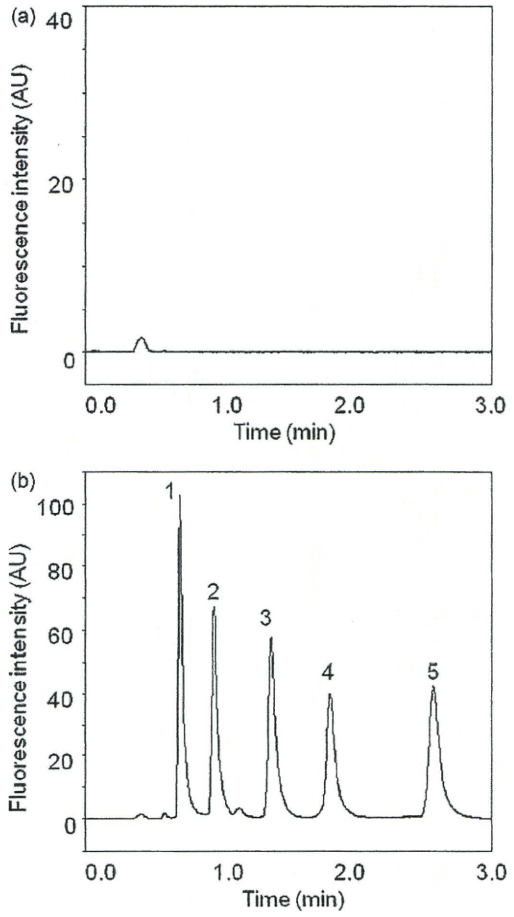

Fig. 3. Chromatograms of (a) HeLa cell homogenate and (b) HeLa cell homogenate spiked with doxorubicin and its metabolites. The chromatographic conditions were the same as in Fig. 2 and are described in Section 2. 1, doxorubicinol; 2, doxorubicin; 3, doxorubicinolone; 4, daunorubicin (internal standard); 5, doxorubicinone.

3.3. Drug recovery

Doxorubicin and its metabolites have a high affinity for cellular constituents [12]. Confocal fluorescence imaging of a HeLa cell that was exposed to doxorubicin for 1 h showed that doxorubicin had preferential affinity for the nucleus (Fig. 4). Drug recovery was assessed by adding doxorubicin, doxorubicinol, doxorubicinolone,

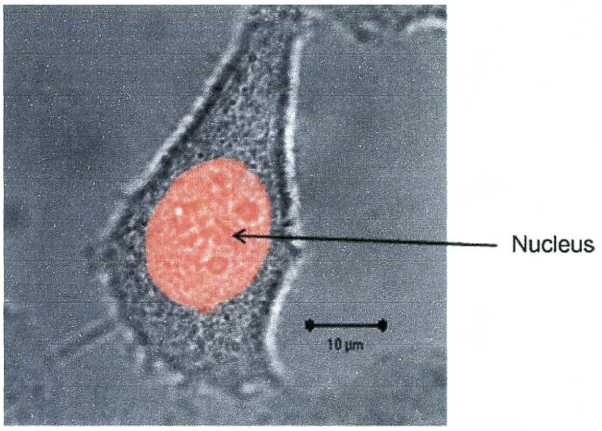

Fig. 4. Intracellular distribution of doxorubicin. HeLa cells were exposed to 1 μg/mL doxorubicin for 1 h, washed, and observed by confocal microscopy. Scale bar: 10 μm.

Table 2
The recovery of doxorubicin and its metabolites from HeLa cell homogenates.

Compound	Recovery rate	
	(%)	R.S.D. (%)
Doxorubicin	102	3.3
Doxorubicinol	105	2.9
Doxorubicinolone	96	1.4
Doxorubicinone	98	2.1

Each compound (1 μg/mL) was added to HeLa cell homogenates, which were then treated as described in Section 2. Mean values for percentage recovery are given ($n=3$).

and doxorubicinone to homogenates of two representative human cancer cell-lines, HeLa cells (derived from human epithelial carcinoma) and HT29 cells (derived from human colon adenocarcinoma grade II) before sample preparation. When the cell homogenate was treated with only methanol and $ZnSO_4$, by a method previously used to study doxorubicin and its metabolites in plasma [9], the percentage recoveries of doxorubicin, doxorubicinol, doxorubicinolone, and doxorubicinone were 84.1 ± 8.2%, 63.2 ± 3.0%, 78.4 ± 3.7%, and 88.7 ± 2.7%, respectively, ($n=3$). Doxorubicinol is harder to recover because it has higher affinity to the cellular constituents, and this affinity to the cellular constituents causes its cytotoxicity [3]. To obtain a higher drug recovery, the cells were lysed by an ultrasonic homogenizer, and the cellular proteins were further digested and solubilized with a combination of Triton X-100 and the endopeptidase proteinase K. Nuclear DNA was hydrolyzed by treatment with DNase I in the presence of divalent cations. Using these enzymatic treatments in accordance with the method of Anderson et al. [4], the recovery dramatically improved (Table 2). Furthermore, for each compound, a satisfactory within-day repeatability was achieved with R. S. D. of ≤ 3.3%, $n=3$.

3.4. Linearity of the calibration plots

We created calibration plots for doxorubicin, doxorubicinol, doxorubicinolone, and doxorubicinone (Fig. 5). The *y*-axis is the ratio of the peak area of each analyte tested to the peak area of the internal standard (daunorubicin), and the *x*-axis is the concentra-

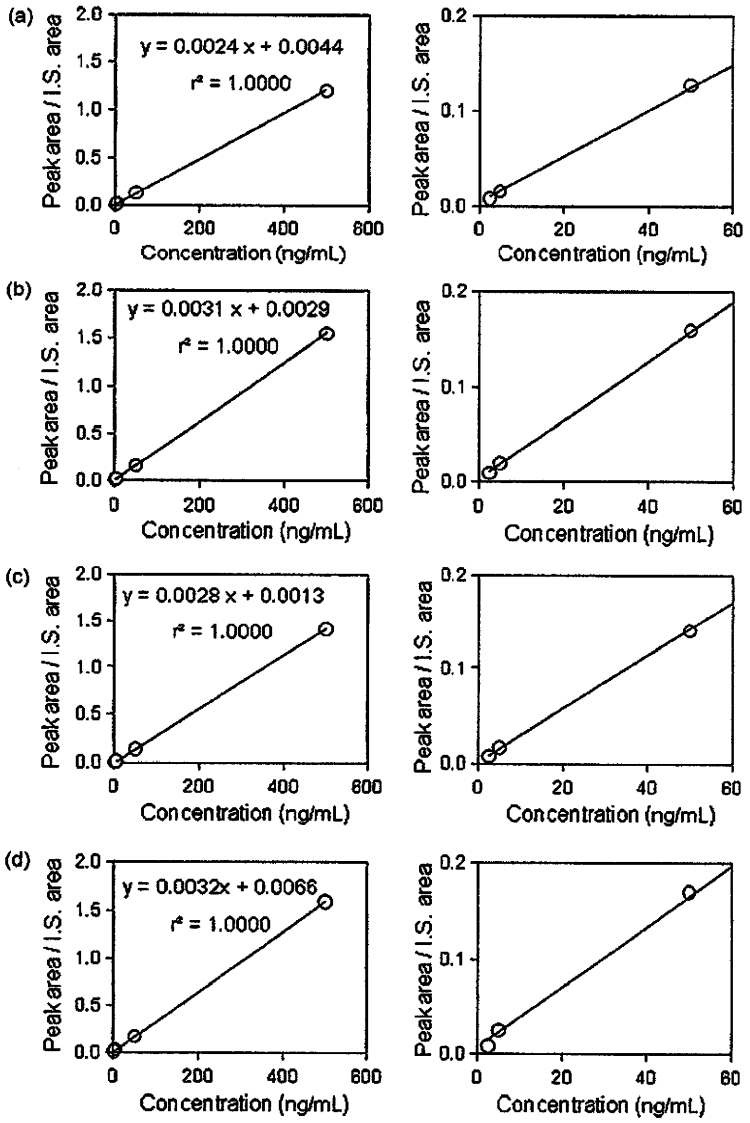

Fig. 5. Linearity of the calibration curves of doxorubicin and its metabolites. Calibration plots for (a) doxorubicin, (b) doxorubicinol, (c) doxorubicinolone, and (d) doxorubicinone. The left and right panels show results for the same HPLC run, but the plots in the right panel focus on the lower concentration ranges. I.S. denotes internal standard.

Table 3
Quantitation of doxorubicin and doxorubicinol in homogenates prepared from doxorubicin-treated cells.

Sample	Doxorubicin (μg/mg cell protein)	Doxorubicinol (μg/mg cell protein)
HeLa cells	3.4 ± 0.55	0.057 ± 0.0060
HT29 cells	3.5 ± 0.38	0.048 ± 0.0029

Cells were treated for 2 h with 10 μg/mL doxorubicin, and cell homogenates were prepared and analyzed, as described in Section 2. Values are given as mean ± S.D. (n (dish number) = 3).

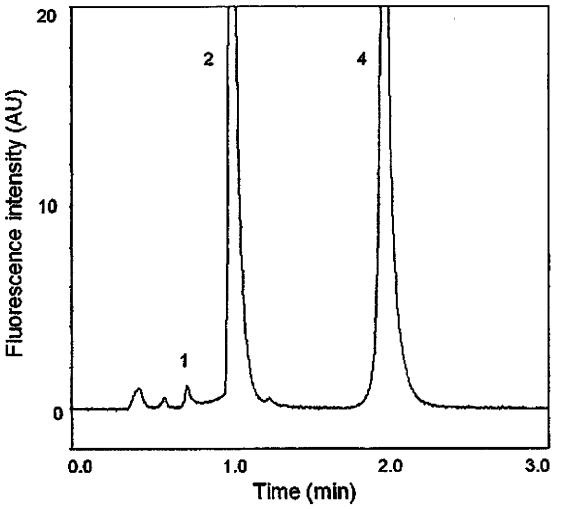

Fig. 6. Chromatogram of cell homogenate obtained 2 h after administration of doxorubicin. HeLa cells were exposed to 10 μg/mL doxorubicin for 2 h. Cell homogenates were then prepared as described in Section 2. 1, doxorubicinol; 2, doxorubicin; 3, daunorubicin (internal standard).

tion of the corresponding analyte. The plots were linear over a wide range of concentrations (r^2 = 1.0; Fig. 5).

3.5. *Quantitative determination of the levels of doxorubicin and its metabolite in cells*

The validated method described above was used for the simultaneous determination of doxorubicin and its metabolites in human cancer cell-lines. HeLa cells and HT29 cells were exposed to 10 μg/mL doxorubicin for 2 h, and then washed with PBS. Chromatograms of the cell homogenates were obtained by UHPLC (Fig. 6). As shown, doxorubicin and one of its metabolites, doxorubicinol, were detected in cell homogenates (Fig. 6). The results of quantitative determination of doxorubicin and doxorubicinol are shown in Table 3. Values are expressed as amounts per 1 mg cellular protein in each dish, due to the diversity of cell numbers for different dishes, and values are given as mean ± S.D. for three dishes of the same cell type. The S.D. values for different dishes of the same cell type were acceptable. Doxorubicinol is produced by cytosolic carbonyl reductase through the NADPH-dependent aldo-keto reduction of a carbonyl moiety in doxorubicin [17]; our results first demonstrated that both human cancer cell-lines, HeLa cells and HT29 cells, produced doxorubicinol from doxorubicin. In contrast, our results showed that deglycosidation at the daunosamine sugar in doxorubicin, which produces doxorubicinone and doxorubicinolone (Fig. 1a) [17], was negligible in these cancer cell-lines (Fig. 6).

New formulation technologies that aim to enhance the effectiveness and safety of anticancer drugs are currently being developed. For instance, long-circulating and sterically stabilized liposomes containing doxorubicin can markedly increase tumor-specific deposition of drugs and have been approved as clinical products [18]. Other carrier systems such as polymer micelles [19,20] are also being developed for use with doxorubicin. In these technologies, effective release of doxorubicin from the carrier into the target cells is important for effectiveness and safety. Direct quantification of the metabolites may facilitate the assessment and comparison of doxorubicin release from carriers, since it is presumed that metabolism of doxorubicin takes place only after its release from the carriers. Analytical methodology that enables the rapid quantification of doxorubicin and its metabolites, particularly in targeted tumor cells, will facilitate the optimization of carrier-based strategies for doxorubicin delivery and will help provide insight into the toxicity and bioavailability of doxorubicin incorporated into carriers such as liposomes or polymer micelles.

4. Conclusions

Our results show that this methodology provides a significant reduction in analysis time and a considerable increase in assay sensitivity. We demonstrated that the method is sensitive enough to quantify the levels of doxorubicin and its metabolite within cells, and we predict that it will greatly facilitate studies of doxorubicin pharmacokinetics and clarify the effect of doxorubicin metabolism on therapeutic outcome at the cellular level. Furthermore, this method can be applied to the evaluation of emerging formulation technologies that are based on encapsulated doxorubicin.

Acknowledgements

The authors are grateful for financial support from the Research on Publicly Essential Drugs and Medical Devices Project (The Japan Health Sciences Foundation), a Health Labor Sciences Research Grant from the Ministry of Health, Labour and Welfare (MHLW), and KAKENHI (21790046) from the Ministry of Education, Culture, Sports, Science, and Technology (MEXT), Japan.

References

[1] G.N. Hortobagyi, Drugs 54 (1997) 1.
[2] A. Di Marco, M. Gaetani, B. Scarpinato, Cancer Chemother. Rep. 53 (1969) 33.
[3] R.D. Olson, P.S. Mushlin, D.E. Brenner, S. Fleischer, B.J. Cusack, B.K. Chang, R.J. Boucek Jr., Proc. Natl. Acad. Sci. U.S.A. 85 (1988) 3585.
[4] A. Anderson, D.J. Warren, L. Slordal, Cancer Chemother. Pharmacol. 34 (1994) 197.
[5] S. Licata, A. Saponiero, A. Mordente, G. Minotti, Chem. Res. Toxicol. 13 (2000) 414.
[6] B. Sundman-Engberg, U. Tidefelt, J. Liliemark, C. Paul, Cancer Chemother. Pharmacol. 25 (1990) 252.
[7] Q. Zhou, B. Chowbay, J. Pharm. Biomed. Anal. 30 (2002) 1063.
[8] J.V. Aspere, O.V. Tellingen, J.H. Beijnen, J. Chromatogr. B: Biomed. Sci. Appl. 712 (1998) 129.
[9] A. Andersen, D.J. Warren, L. Slordal, Ther. Drug Monit. 15 (1993) 455.
[10] S. Shinozawa, Y. Mimaki, Y. Araki, T. Oda, J. Chromatogr. 196 (1980) 463.
[11] L.M. Rose, K.F. Tillery, S.M. el Dareer, D.L. Hill, J. Chromatogr. 425 (1988) 419.
[12] A. Andersen, H. Holte, L. Slordal, Cancer Chemother. Pharmacol. 44 (1999) 422.
[13] M.E. Swartz, J. Liq. Chromatogr. Relat. Technol. 28 (2005) 1253.
[14] L. Novakova, H. Vlckova, Anal. Chim. Acta 656 (2009) 8.
[15] N. Sun, G. Lu, M. Lin, G. Fan, Y. Wu, Talanta 78 (2009) 506.
[16] K.E. Maudens, C.P. Stove, W.E. Lambert, J. Sep. Sci. 31 (2008) 1042.
[17] S. Takanashi, N.R. Bachur, Drug Metab. Dispos. 4 (1976) 79.
[18] M.E.R. O'Brien, N. Wigler, M. Inbar, R. Rosso, E. Grischke, A. Santoro, R. Catane, D.G. Kieback, P. Tomczak, S.P. Ackland, F. Orlandi, L. Mellars, C. Tendler, Ann. Oncol. 15 (2004) 440.
[19] M. Yokoyama, T. Okano, Y. Sakurai, S. Fukushima, K. Okamoto, K. Kataoka, J. Drug Target. 7 (1999) 171.
[20] T. Nakanishi, S. Fukushima, K. Okamoto, M. Suzuki, Y. Matsumura, M. Yokoyama, T. Okano, Y. Sakurai, K. Kataoka, J. Control. Release 74 (2001) 295.

RESEARCH ARTICLE

Stabilization of Liposomes in Frozen Solutions Through Control of Osmotic Flow and Internal Solution Freezing by Trehalose

KEN-ICHI IZUTSU, CHIKAKO YOMOTA, TORU KAWANISHI

National Institute of Health Sciences, Setagaya-ku, Tokyo 158-8501, Japan

Received 22 September 2010; revised 7 December 2010; accepted 25 January 2011

Published online in Wiley Online Library (wileyonlinelibrary.com). DOI 10.1002/jps.22518

ABSTRACT: The purpose of this study was to elucidate the effect of trehalose distribution across the membrane on the freeze-related physical changes of liposome suspensions and their functional stability upon freeze–thawing. Cooling thermal analysis of 1,2-dipalmitoyl-*sn*-glycero-3-phosphocholine liposome suspensions showed exotherm peaks of bulk (−15°C to −25°C) and intraliposomal (approx. −45°C) solution freezing initiated by heterogeneous and homogeneous ice nucleation, respectively. The extent of the intraliposomal solution freezing exotherm depended on liposome size, lipid composition, cosolutes, and thermal history, suggesting that osmotic dehydration occurred due to the increasing difference in solute concentrations across the membrane. A freeze–thawing study of carboxyfluorescein-encapsulated liposomes suggested that controlling the osmotic properties to avoid the freeze-induced intraliposomal solution loss either by rapid cooling of suspensions containing trehalose in both sides of the membrane (retention of the intraliposomal supercooled solution) or by cooling of suspensions containing trehalose in the extraliposomal media prior to freezing (e.g., osmotic shrinkage) led to higher retention of the water-soluble marker. Evaluation and control of the osmotically mediated freezing behavior by optimizing the formulation and process factors should be relevant to the cryopreservation and freeze-drying of liposomes. © 2011 Wiley-Liss, Inc. and the American Pharmacists Association J Pharm Sci

Keywords: liposomes; formulation; stabilization; thermal analysis; osmosis; calorimetry (DSC); excipients; freeze-drying

INTRODUCTION

The increase in the variety and clinical relevance of liposomal formulations has enhanced the importance of the freezing and freeze-drying processes for the distribution and long-term storage of the drug delivery systems that are not chemically and/or physically stable enough as aqueous suspensions.[1–4] These processes, however, expose the lipid systems to various stresses including ice growth, pH change, concentration of the surrounding solutes, and dehydration that often damage their structural integrity and pharmaceutical functions [e.g., release of active pharmaceutical ingredients (APIs)] of liposomes. Retaining water-soluble APIs is a particular challenge for development of liposome formulations.[1] Formulation and process design that are based on an understanding of the freeze-related stresses and required stabilization mechanisms should improve the stability of various liposome pharmaceuticals.[1–3]

Disaccharides (e.g., trehalose and sucrose) and some amino acids have been applied to protect the lipid systems from chemical and physical changes during freeze–thawing (cryoprotectants) and freeze-drying (lyoprotectants).[1,3] The stabilization of liposomes by disaccharides is explained mainly by three mechanisms. Some saccharides substitute the water molecules necessary to retain the supramolecular phospholipid assembly through molecular interactions with hydrophilic phospholipid head groups (water substitution).[5–7] The saccharides also form highly viscous amorphous freeze-concentrated phases and dried solids that prevent direct contact between liposome vesicles (bulking).[1,8,9] The reduced mobility of the surrounding molecules helps improve the chemical and physical stability of liposomes (vitrification). Use of the stabilizers is mostly dependent on empirical trial and error through analysis of the morphological (e.g., size) and functional (e.g., API or marker

Correspondence to: Ken-ichi Izutsu (Telephone: +81-3-3700-1141; Fax: 81-3-3707-6950; E-mail: izutsu@nihs.go.jp)

Journal of Pharmaceutical Sciences

retention) traits of the resulting suspensions or dried solids.

Longstanding cryopreservation studies of living cells and microorganisms provide precepts valuable for the protection of liposomes against the freeze-induced stresses.[10–14] The cooling of cell and liposome suspensions induces the freezing of bulk solutions initiated by heterogeneous ice nucleation at the surface of containers or impurities (−5°C to −25°C) and the freezing of spatially restricted internal solutions initiated by homogeneous (spontaneous) ice nucleation (−25°C to −45°C).[15–21] The bulk solution freezing and the accompanying significant concentration of solutes surrounding the living cells and liposomes induce osmotic stress that removes the internal solution before they freeze, leading to morphological changes observable by microscopic methods (e.g., optical microscope and cryo-transmission electron microscopy).[21,22] Because the intracellular ice formation (IIF) is widely recognized to cause lethal damage through disordering of the complex membrane and intracellular structure (e.g., organelle), cryopreservation of the living cells and microorganisms is usually performed in two ways that prevent IIF, namely by slow cooling of suspensions containing extracellular solutes (cell dehydration) and by rapid cooling of the suspensions containing high-concentration membrane-permeating solutes [e.g., dimethyl sulfoxide (DMSO), cytoplasm vitrification].[12] On the contrary, only limited studies have been performed on the stabilization of liposomes taking various freezing-related physical changes into account.[17,23–25]

The purpose of this study was to elucidate the effect of intra- and extraliposomal trehalose on the freeze-related physical changes and functional stability of liposomes during freeze–thawing. The effect of saccharide distribution across the membrane on the stability of liposomes is of particular interest for formulation purposes because the liposome preparation methods significantly affect allocation of the nonpermeating solutes. Different solute concentrations across the membrane induce osmotic flow that shrinks or swells the liposomes in the aqueous suspensions.[4,22,26] Literature claims the requirement of disaccharides on both sides of the membrane to protect liposomes from freezing- and lyophilization-related stresses (e.g., addition before extrusion).[8] Recent reports suggested that the rational setting of different intra- and extraliposomal trehalose concentrations confers better stabilization.[1,27] Effect of trehalose on the freeze-related physical phenomena (e.g., freeze-induced dehydration and intraliposomal solution freezing) and functional stability of liposomes were studied mainly through thermal analysis and through the retention of encapsulated carboxyfluorescein (CF).[27,17]

MATERIALS AND METHODS

Materials

Chemicals obtained from the following sources were used without further purification: 1-palmitoyl-2-oleoyl-*sn*-glycero-3-phosphocholine (POPC), 1,2-dimyristoyl-*sn*-glycero-3-phosphocholine (DMPC), 1,2-dipalmitoyl-*sn*-glycero-3-phosphocholine (DPPC), and 1,2-distearoyl-*sn*-glycero-3-phosphocholine (DSPC) (NOF Co., Tokyo, Japan); trehalose dihydrate, glucose, sucrose, and 5(6)-CF (Sigma–Aldrich Co., St. Louis, Missouri); DMSO, xylitol, and glycerol (Wako Pure Chemical Co., Osaka, Japan); and dextran 4000–6000 (Serva Electrophoresis GmbH, Heidelberg, Germany).

Preparation of Liposome Suspensions

Phospholipid films were obtained by drying their solution in a chloroform and methanol mixture (2:1) under vacuum at temperatures above the main transition temperature (T_m). Liposome suspensions were prepared by using a hand-held extruder (Avanti Polar Lipids, Alabaster, Alabama). The films hydrated by 10 mM Tris–HCl buffer (6%, w/w; pH 7.4) were extruded 12 times through a polycarbonate membrane filter (0.1–0.8 μm pore, 0.2 μm unless otherwise mentioned; Whatman, Maidstone, UK) while maintaining the apparatus at room temperature (POPC) or at temperatures 10 to 15°C higher than the T_m of the respective lipids. The DPPC liposomes extruded through the smaller pore membranes (0.1 and 0.2 μm) were reported to have a unilamellar structure, whereas those extruded through the larger pore membranes (0.4 and 0.8 μm) contained increasing ratios of multilamellar vesicles.[29,30] The term "0.2 μm liposome" will be used in the text given below to denote samples prepared by extrusion through the respective pore size membranes.

Some liposome suspensions containing the excipients predominantly in the extraliposomal media were prepared by adding the excipients approximately 30 min prior to the thermal analysis and freeze–thawing experiments. Those containing excipients in both the inside and outside of the membranes were prepared by the extrusion of lipids hydrated with the excipient-containing solutions. Some suspensions were eluted through Sephadex G-25 desalting columns (PD-10; GE Healthcare Bio-Sciences AB, Uppsala, Sweden) equilibrated with the Tris–HCl buffer to obtain samples containing the excipient mainly in the intraliposomal solutions. The concentrations of DPPC in the column-eluted suspensions were obtained by phosphorous assay.[31] Measurement of the DPPC concentrations in the liposome suspensions indicated that approximately 90% of the liposomes passed through the Sephadex columns.

DOI 10.1002/jps

Thermal Analysis

Thermal analysis of the frozen liposome suspensions was performed by using a differential scanning calorimeter (DSC Q10; TA Instruments, New Castle, Delaware) equipped with a refrigerating system and data processing software (Universal Analysis 2000, TA Instruments). Aliquots [10 μL, 4% (w/w) lipid] of suspensions in hermetic aluminum cells were cooled from 25°C to −70°C at varied speeds (1–10°C/min) and then heated to 25°C at a scanning rate of 5°C/min. The intensity of the intraliposomal solution freezing exotherm was shown as their ratio to the lipid content (J/g lipid). Some DPPC liposome suspensions were heat-treated at 45°C for 3 min before the cooling scan. The cooling scan of some suspensions were paused at certain temperatures (−10°C to −35°C) and maintained those temperatures for 30 or 60 min before further cooling to study the effect of low temperature storage on the physical changes. The column-eluted liposome suspensions were subjected to thermal analysis without the concentration adjustment. The homogeneous ice formation exotherms of these suspensions were calculated using the phosphate concentration data.

Measurement of Liposome Size by Dynamic Light Scattering

The size distribution of liposomes suspended in the Tris–HCl buffer (0.08% DPPC, 25°C) was determined using a dynamic light scattering (DLS) spectrophotometer (Photal DLS-7100SL; Otsuka Electronics Co., Osaka, Japan) with a He–Ne laser (632.8 nm) and a scattering angle (90°; 50 scans).

CF Retention Study

Dried DPPC films were hydrated with solutions containing 25 mM 5(6)-CF, 10 mM Tris–HCl buffer, and 0% or 12% trehalose, adjusted to pH 7.4 by NaOH. The CF-loaded vortexed multilamellar liposome suspensions (6% lipid, w/w) were prepared by extrusion through a 0.2-μm pore filter, and then eluted through the Sephadex G-25 column equilibrated with the buffer or trehalose-containing buffer. Freeze–thawing of the suspension was performed using the DSC system while the thermal profiles were simultaneously monitored. Aliquots of the liposome suspensions (10 μL, 4% DPPC, w/w) in unsealed aluminum pans were cooled to −35°C or −70°C at varied cooling speeds (1–10°C/min), and then heated to 25°C at 10°C/min on the DSC furnace. The freeze–thawed liposome suspensions were diluted by adding the Tris–HCl buffer or trehalose-containing buffer solutions (10 mL) in the glass tubes. The mildly agitated liposome suspensions underwent fluorescence measurement using a spectrometer (FP-6500; JASCO Corp., Tokyo, Japan). After the initial fluorescence measurements of the suspensions (2 mL) at 460 nm (excitation) and 550 nm (emission), those of the membrane-perturbed liposome suspensions were obtained by the addition of aliquots (20 μL) of Triton X-100. The CF leakage ratio was calculated using the following equation:

$$\%\,\text{Leakage} = \frac{\text{Initial fluorescence of treated sample} - \text{initial fluorescence of control}}{(\text{Final fluorescence of treated sample} - \text{initial fluorescence of control})} \times 100$$

RESULTS AND DISCUSSION

Freeze-Induced Changes in Liposome Suspensions

Figure 1 shows a thermogram of a frozen DPPC liposome suspension (4% in 10 mM Tris–HCl buffer, 0.2 μm) cooled at 5°C/min. The suspension showed a large exothermic peak of the freezing of the bulk solution (heterogeneous ice nucleation) at approximately −20°C and a smaller second exothermic peak of the freezing of the intraliposomal solution (homogeneous ice nucleation) at approximately −45°C.[15,17,32] The lower temperature exotherm disappeared by prior addition of a membrane-perturbing surfactant (1% Triton X-100), which supported the aforementioned definition of the peak rather than other interpretations (e.g., freezing of phosphatidylcholine headgroups) of the exotherm (data not shown).[33] The temperature

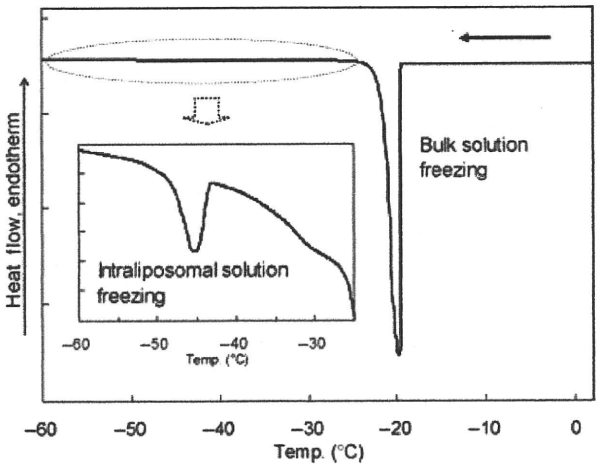

Figure 1. Cooling thermogram of a frozen DPPC liposome suspension. An aliquot (10 μL) of liposome suspension (4% lipid, w/w) in Tris–HCl buffer (10 mM, pH 7.4) was cooled from room temperature to −70°C at 5°C/min.

of the bulk solution freezing peak varied greatly between the scans. Some suspensions also showed a broad exotherm at approximately −30°C. The exotherm suggested the freezing of solutions released from the liposomes (dehydration) and/or freezing of the internal solutions initiated by external ice crystals that penetrated through the membrane.[12,16,34] The varied shape and overlapping of the peak with the large bulk solution freezing exotherm made further characterization difficult in this study. The frozen liposome suspensions showed only a gradual shift of the thermogram before the large ice melting endotherm during their heating scans (data not shown). DLS measurement of the DPPC liposome suspensions indicated a mean diameter of 203.9 ± 10.6 nm before the thermal analysis (three different preparations). Standard deviation of the liposome size obtained in each measurement was within 5% of the average value.

The effects of cooling speeds on the internal solution freezing exotherm of liposomes differing in size and lipid composition are shown in Figure 2. Slower cooling of the DPPC liposome suspension (0.2 μm) reduced the exotherm, indicating loss of the supercooled intraliposomal solution during the scan (Fig. 2a; 1 –2°C/min). The extraliposomal ice growth and concomitant concentration of solutes should generate osmotic forces that induce water evacuation from liposomes. Reported freeze-induced morphological rearrangement into multilamellar liposomes may also reduce the intraliposomal solution content.[4] The width of the bulk solution freezing peak got narrower in the slower cooling, suggesting a certain time required for the ice growth (data not shown). On the contrary, the limited effect of the cooling speed on the peak width of the intraliposomal solution freezing exotherm suggested independent ice formation in the individual liposomes. A certain amount of the intraliposomal solution interacting (hydrating) with the membrane lipid and/or solute molecules should remain unfrozen even below the intraliposomal solution freezing temperature.[11,11]

Reduction of the intraliposomal solution freezing exotherm was more apparent in the DPPC liposome suspensions temporarily (30 min) kept at temperatures between the bulk and the intraliposomal solution freezing during the cooling scan (Fig. 3). The finding that the intraliposomal solution freezing exotherm of a suspension held at −25°C was smaller than those of suspensions held at −30°C or −35°C suggested faster loss of the supercooled solutions in the temperature range just below the bulk solution freezing. Longer exposure to the temperature range should be one of the reasons for the reduction in the exotherms with the slower cooling. On the contrary, holding the suspension at a temperature above the bulk solution freezing temperature showed no apparent effect on the intraliposomal solution freezing

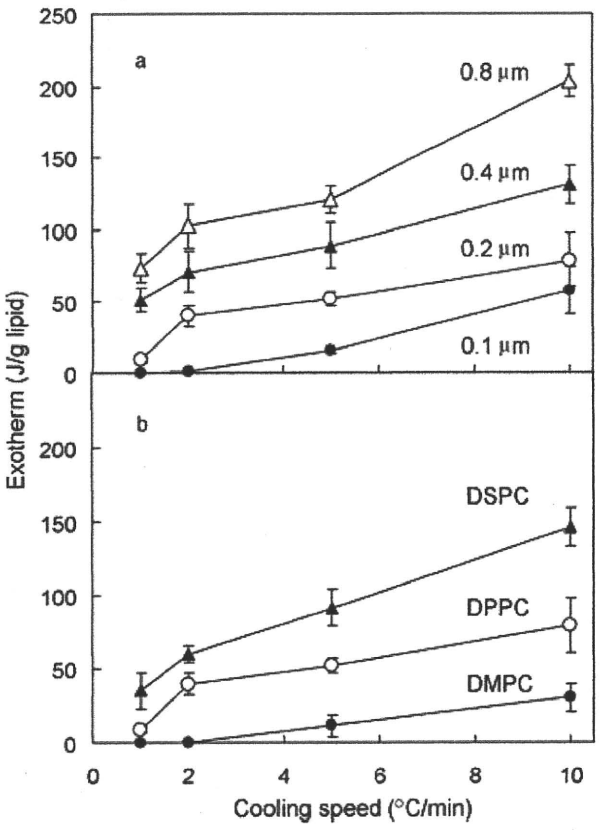

Figure 2. Effects of cooling speed on internal solution freezing exotherm of liposome suspensions with differing (a) extrusion membrane pore sizes (DPPC; 0.1 μm: •, 0.2 μm: ○, 0.4 μm: ▲, and 0.8μm: △) and (b) lipid compositions (0.2 μm; DMPC: •, DPPC: ○, and DSPC: ▲). Aliquots of liposome suspensions (10 μL, 4% lipid in 10 mM Tris–HCl buffer) were cooled at 1–10°C/min (average ± SD, $n = 3$).

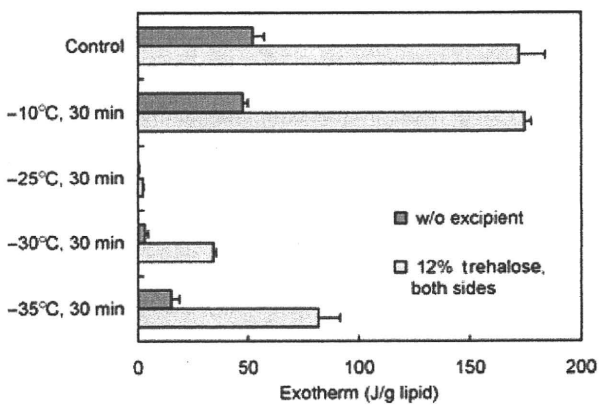

Figure 3. Effect of low temperature holding on internal solution freezing exotherms of DPPC liposome suspensions containing trehalose (0% or 12%, w/w) on both sides of the membrane (10 μL, 4% lipid in Tris–HCl buffer, 0.2 μm). The suspensions were held at different temperatures (−10°C to −35°C) for 30 min during cooling scans at 5°C/min.

DOI 10.1002/jps

exotherm. The absence of apparent osmotic driving force may explain the limited effect of storage at above the bulk solution freezing temperature.

The DPPC liposome suspensions extruded through larger pore size filters (e.g., 0.4 and 0.8 μm) showed larger intraliposomal solution freezing exotherms (Fig. 2a). Factors including the possibility of higher initial solution contents per lipid weight, limited membrane disordering associated with the curvature, and slower dehydration due to the increase in multilamellar membranes would explain the large exotherms. Liposomes composed of phosphatidylcholines of different acyl chain lengths showed retention of the intraliposomal solution down to the homogeneous ice formation temperature in the order of DMPC < DPPC < DSPC (Fig. 2b). The intraliposomal solution freezing exotherm was not observed in the thermal analysis of POPC liposome suspensions (data not shown). All the liposome membranes are below their T_m (POPC: −5°C, DMPC: 24°C, DPPC: 41°C, DSPC: 54°C) at the bulk solution freezing temperature.[35] Possible differences in the membrane fluidity and rigidity would cause the freeze-induced dehydration to vary.

Effect of Trehalose Distribution on Freezing Profiles of Liposome Suspensions

The effects of intra- and extraliposomal trehalose on the freezing behavior of liposome suspensions were studied. The DPPC liposome suspensions containing trehalose on both sides of the membrane showed larger intraliposomal solution peaks that suggest reduced solution loss upon the bulk solution freezing. For example, cooling of the 0.2 μm DPPC suspensions at 10°C/min resulted in exotherms of approximately 80 and 200 J/g lipid, respectively, in the absence and presence of trehalose (Figs. 2 and 4). The addition of trehalose also lowered the peak temperature of the exotherm (approx. 3°C at 12% trehalose, w/w).[18,34] The trehalose-containing liposome lost a larger amount of the internal supercooled solution during the slower cooling of the suspensions. Temporary pausing of the cooling scan suggested a faster loss of the supercooled solution near the bulk solution freezing temperature (−25°C), also in the trehalose-containing liposome suspensions (Fig. 3). The addition of various low-molecular-weight saccharides and polyols to both sides of the lipid membrane increased the freezing exotherm of the intraliposomal solutions, suggesting that slower freeze-induced dehydration occurred due to the colligatively determined osmotic effect (Fig. 5). The limited effect of dextran on the exotherm could be explained by its lower molar concentration and its possible exclusion from the vicinity of the liposomes in the freeze-concentrated nonice phase.[36] The large (0.4 and 0.8 μm) or lower fluidity (DSPC) liposomes retained higher amounts of

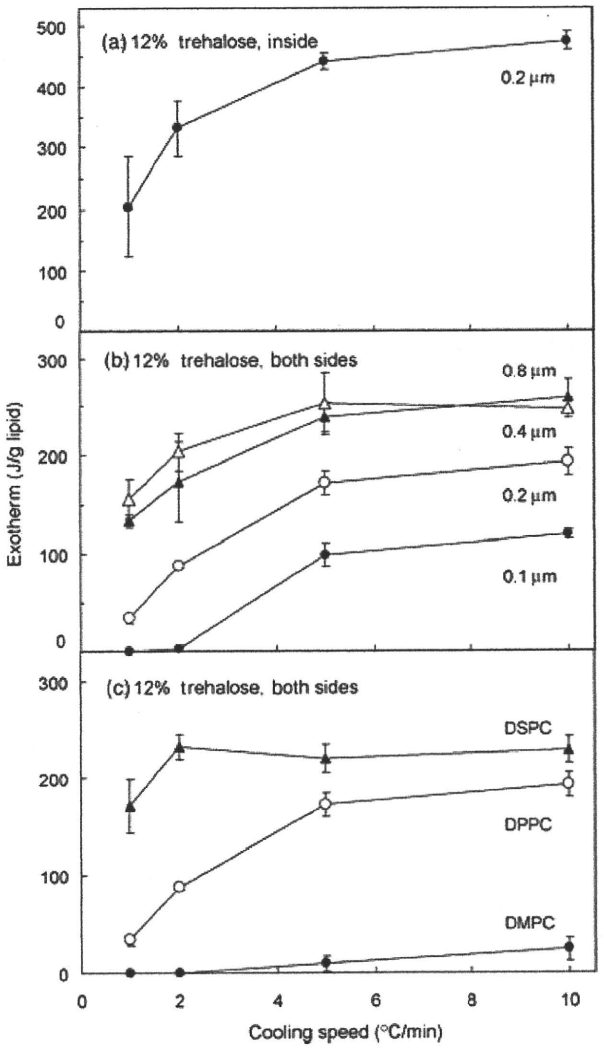

Figure 4. Internal solution freezing exotherms of liposome suspensions containing trehalose (12%, w/w) on (a) the inside and (b, c) both sides of liposomes. Aliquots of suspensions (10 μL, 4% lipid in 10 mM Tris–HCl buffer) containing liposomes with (b) differing extrusion membrane pore sizes (DPPC; 0.1 μm: •, 0.2 μm: ○, 0.4 μm: ▲, and 0.8 μm: △) and (c) lipid compositions (0.2 μm; DMPC: •, DPPC: ○, and DSPC: ▲) were cooled at 1–10°C/min (average ± SD, $n = 3$).

freezable intraliposomal solution in the presence of trehalose on both sides of the membrane (Figs. 4b and 4c).

1,2-Dipalmitoyl-*sn*-glycero-3-phosphocholine liposomes containing trehalose on one side of the membrane showed different freezing behaviors. The addition of higher concentration trehalose to the extraliposomal media reduced the intraliposomal solution freezing exotherm (Fig. 6). The difference in the osmotic pressures across the membrane should induce solution flow that dehydrates the liposomes both prior to cooling and after the bulk solution freezing. The

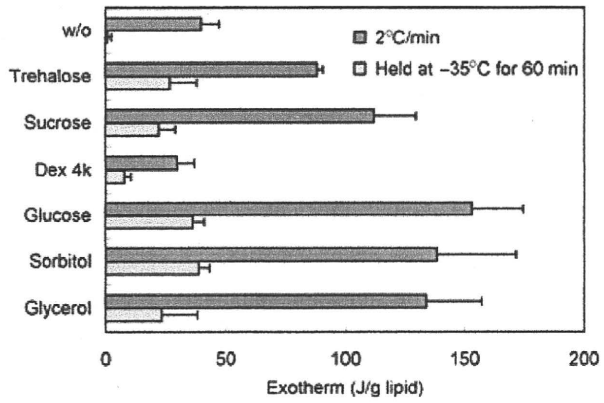

Figure 5. Effect of various extraliposomal solutes (12%, w/w) on internal solution freezing exotherms of DPPC liposome suspensions (10 μL, 4% lipid in 10 mM Tris–HCl buffer, 0.2 μm) obtained via cooling scans at 2°C/min (average ± SD, $n = 3$). Some suspensions were held at −35°C for 60 min during the scan.

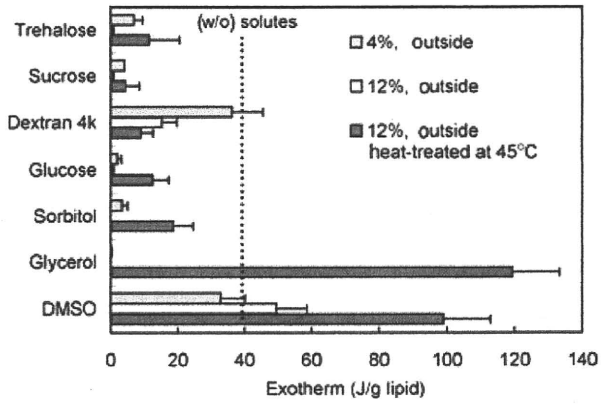

Figure 7. Effect of various extraliposomal solutes (4% and 12%, w/w) on internal solution freezing exotherms of DPPC liposomes obtained via cooling scans of suspensions (10 μL, 4% DPPC in 10 mM Tris–HCl buffer, 0.2 μm) from room temperature to −70°C at 2°C/min. Some suspensions were heat-treated at 45°C for 3 min before the cooling analysis (average ± SD, $n = 3$).

absence of a broad exotherm between the bulk and intraliposomal solution freezing peaks suggested that liposome dehydration before the bulk solution freezing (e.g., osmotic shrinkage) had occurred rather than the freeze-induced dehydration (data not shown).

Other low-molecular-weight saccharides and polyols in the extraliposomal media also reduced the intraliposomal solution freezing exotherms of the DPPC liposomes (Fig. 7). The extraliposomal dextran showed smaller effect to reduce the exotherm compared with the lower-molecular-weight excipients. Prior heat treatment of the liposome suspensions at above T_m of DPPC (45°C, 3 min), apparently increased the intraliposomal solution freezing exotherm of the suspensions containing the externally added glycerol or DMSO. Membrane disordering at and above the transition temperature should allow an influx of the highly permeable small solute molecules, and should, thus, reduce the osmotic effect that dehydrates the liposomes.

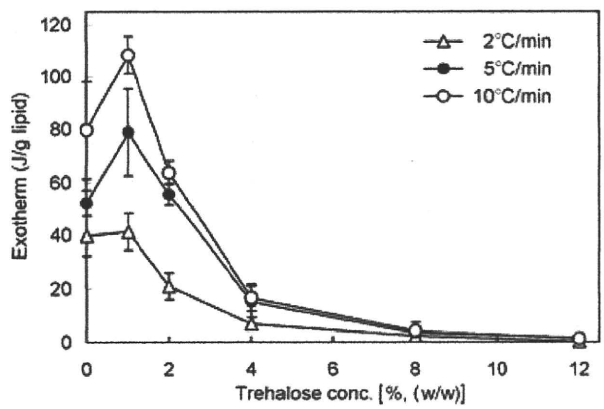

Figure 6. Effect of extraliposomal trehalose (0%–12%, w/w) on internal solution freezing exotherms of DPPC liposome suspensions (10 μL, 4% lipid in 10 mM Tris–HCl buffer, 0.2 μm) obtained by cooling at 2°C/min (Δ), 5°C/min (•), or 10°C/min (○)(average ± SD, $n = 3$).

The effect of intraliposomal trehalose on the freezing behavior of DPPC liposomes was also studied (Fig. 4a). The suspensions containing trehalose predominantly inside the liposomes showed apparently larger exotherms than those of other suspensions. The absence of the baseline shift at the trehalose transition temperature of maximally freeze-concentrated solutes (T_g') in the heating scan confirmed the low trehalose concentration outside the liposomes (data not shown). Liposomes prepared by extrusion often contain an amount of internal solution that was insufficient to fill the completely spherical structure, which allows inward water flow across the membrane upon exposure of liposomes to lower osmolarity solutions.[37] An increase in the intraliposomal solution content due to osmotic swelling in the initial suspension and limited freeze-induced dehydration can explain the larger ice formation peaks. These results indicated that the osmotic effect made a significant contribution to the freezing behavior of liposomes.

Kinetic stability of the trehalose-containing supercooled intraliposomal solutions was studied to elucidate their relevance in freeze-drying process (Fig. 8). Some liposome suspensions (e.g., trehalose-containing 0.8 μm DPPC liposome) showed small but apparent intraliposomal solution freezing peaks in the scans after a slower cooling (0.5°C/min) followed by being held at −35°C (180 min). The result suggested that some liposomes retain certain amount of internal solutions during freezing segment of pharmaceutical formulation lyophilization usually

DOI 10.1002/jps

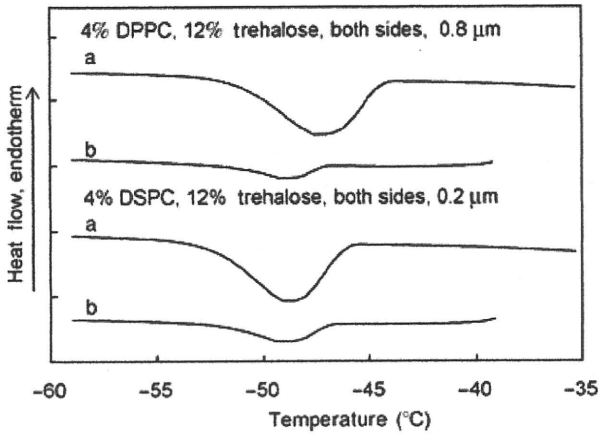

Figure 8. Cooling thermograms of DPPC (0.8 μm) and DSPC (0.2 μm) liposome suspensions containing trehalose (12%, w/w) on both sides of the membrane (10 μL, 4% lipids in 10 mM Tris–HCl buffer). The suspensions were cooled at 5°C/min (a) from room temperature or (b) after slow cooling (0.5°C/min) with a temporary pause at −35°C (180 min).

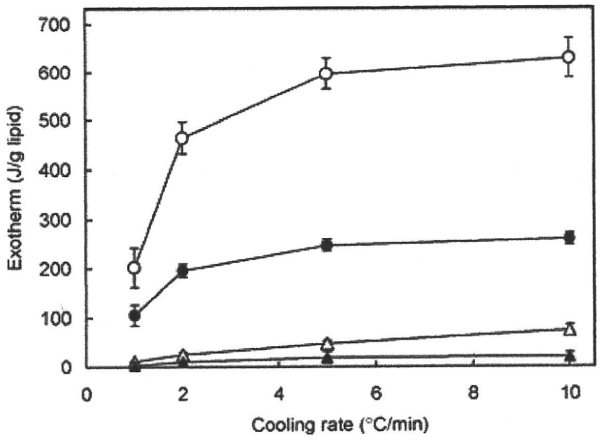

Figure 9. Internal solution freezing exotherms of carboxyfluorescein (25 mM)-containing DPPC liposome suspensions (10 μL, 4% DPPC in 10 mM Tris–HCl buffer, 0.2 μm) without (△) or with 12% trehalose on the outside (▲), inside (○), or both sides (●) of the liposome membrane scanned from room temperature at 1–10°C/min (average ± SD, $n = 3$).

performed via slow cooling (e.g., 0.2–0.5°C/min) down to −35°C to −50°C on the lyophilizer shelf.[38,39] The lower product temperature during the process should lead to freezing of the intraliposomal solutions by the homogeneous ice nucleation mechanism.

Effect of Freeze–Thawing on CF-Encapsulated Liposomes

The relationship between trehalose-induced changes in the liposome freezing behavior and functional stability of liposomes upon freeze–thawing was studied (Figs. 9 and 10). The CF-loaded DPPC liposomes were subjected to thermal analysis and freeze–thawing marker-retention study (a) without trehalose, (b) with trehalose on both sides of the membrane, (c) with trehalose in the intraliposomal solution, or (d) with trehalose in the extraliposomal media. A lower concentration (25 mM; approx. 0.94%, w/w) of CF compared with those in other retention studies (e.g., 100 mM) was used for the experiment to reduce its osmotic effect on the freezing behavior of the liposomes. A thermal transition ($T_g' = -36.2$°C) and absence of other peaks in the heating process of a frozen CF solution (25 mM in Tris–HCl buffer, pH 7.4) indicated that the solute was in a noncrystalline state in the freeze-concentrated phase. The CF-loaded liposome suspensions showed small intraliposomal solution freezing exotherms essentially identical to those of the marker-free samples in the absence of trehalose (Figs. 2 and 9). The liposomes lost a large fraction of the markers upon freeze–thawing of the trehalose-free suspensions cooled down to −35°C (below bulk solution freezing temperature) and −70°C (below intraliposomal solution freezing temperature) at all speeds (Fig. 10).

The DPPC liposomes containing trehalose on both sides of the membrane retained higher intraliposomal solution and encapsulated CF contents under faster cooling (5 and 10°C/min). Small changes of the marker retention in the fast cooling of the suspensions down to −35°C and −70°C suggested that the intraliposomal freezing by itself is not a main cause of the severe marker leakage, at least in the presence of trehalose. A large loss of the intraliposomal solution and

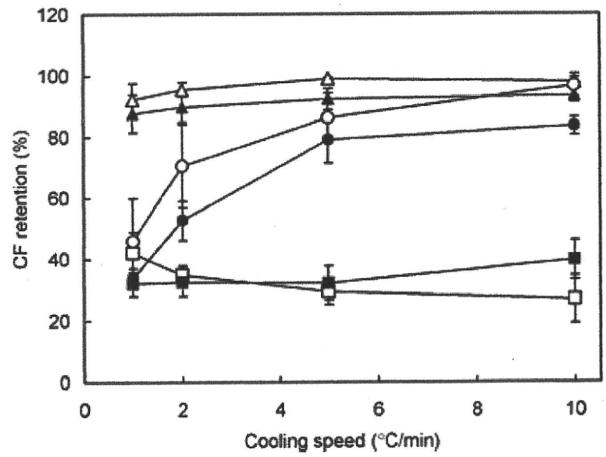

Figure 10. Effect of freeze–thawing on retention of carboxyfluorescein (CF) encapsulated in DPPC liposomes. Aliquots of CF (25 mM)-containing DPPC liposome suspension (10 μL, 4% lipid in 10 mM Tris–HCl buffer, 0.2 μm) without (□, ■) or with 12% trehalose on the outside (△, ▲) or both sides (○, ●) of the liposome membrane were cooled from room temperature to −35°C (open symbols) or −70°C (closed symbols) at 1–10°C/min, and then heated at 10°C/min (average ± SD, $n = 3$).

an accompanying apparent leakage of the marker in the slowly cooled suspensions suggested that membrane damage had occurred that allowed outbound flow of the marker-containing solution during the freezing process. Experiencing the fast-dehydrating temperature range twice in a freeze–thawing cycle should explain the larger change in marker retention compared with that of the intraliposomal freezing exotherm obtained in some cooling procedures. Suspensions containing CF and trehalose only in the intraliposomal solution also showed large intraliposomal solution freezing exotherms (Figs. 4a and 9). Solidification of the suspensions upon freeze–thawing, which hindered the CF retention measurement, confirmed the requirement of trehalose in the extraliposomal media (data not shown).[16]

The externally added trehalose (12%) reduced the CF leakage from the DPPC liposomes upon freeze–thawing at all cooling speeds. The suspensions showed a minor exotherm during the intraliposomal solution freezing. Possible osmotic shrinkage prior to freezing is the likely explanation for the limited internal solution content and the high retention of the encapsulated marker.[4,22,26] The addition of trehalose to the extraliposomal media (12%) induced leakage of less than 1% of the encapsulated CF at room temperature (data not shown).[40] Changes in the color of CF-containing liposome suspensions from yellow to orange by the extraliposomal trehalose suggested an increasing intraliposomal marker concentration due to outbound water flow through membrane diffusion (osmotic shrinkage). The lower intraliposomal solution contents should lead to the limited freeze-induced dehydration and membrane damage. The extraliposomal saccharides should also protect liposomes from membrane injury due to the growing ice surface, an excess concentration of unfavorable solutes (e.g., inorganic salts), and direct contact of concentrated liposome membranes as spacer.[40,39]

Liposome Stabilization by Control of the Osmotic Flow and Internal Freezing

The results indicated varied effect of trehalose on the freezing behavior and functional stability of liposomes upon freeze–thawing depending on its distribution across the membrane. A schematic flow of the liposome freezing behavior is shown in Figure 11. Understanding the physical changes and the encountering stresses should be relevant for strategic stabilization in freeze–thawing and freeze-drying of liposomes. Liposomes prepared by extrusion often do not contain sufficient solutions to fill the spherical structure.[37,41] Exposure of the liposomes either increases (e.g., osmotic swelling in hypotonic media) or decreases (e.g., osmotic shrinkage in hypertonic media) the internal solution content via water diffusion through the membranes. The bulk and intraliposomal solutions freeze at different temperatures, as the processes are initiated by the heterogeneous and homogeneous ice nucleation mechanisms, respectively. The freeze-induced osmotic dehydration and the intraliposomal solution freezing initiated by membrane-penetrating ice crystals should reduce intraliposomal solution content that freeze at the homogeneous ice nucleation temperature.[12,16,34,42] Accordingly, the intraliposomal solution should be in the dehydrated, supercooled, or frozen states in the frozen suspensions depending on the formulation and process factors. The absence of crystallizing solutes (e.g., mannitol) allowed observation of the freeze-induced physical changes through thermal analysis.[28]

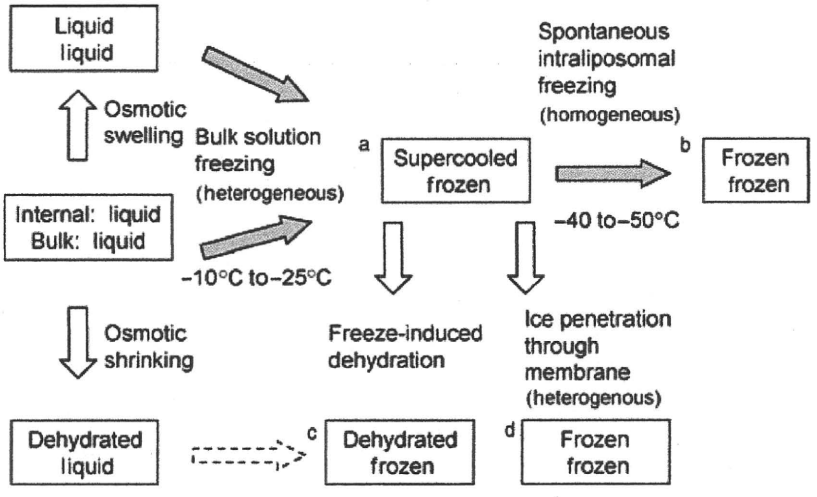

Figure 11. Schematic freezing behaviors of extruded liposome suspensions. The upper and lower rows in each box denote the physical state of the intraliposomal and bulk solutions, respectively. Boxes (a) to (d) indicate suggested physical states of frozen liposome suspensions.

DOI 10.1002/jps

Each step of the freeze-related physical changes induces stresses that affect the stability of liposomes. The growing ice during the bulk and intraliposomal solution freezing should physically damage the liposome membranes. It is possible that the freeze-induced large difference in the osmotic pressure causes larger membrane damage in the DPPC liposomes than in the living cells because of their lower hydraulic permeability, leading to a dehydrating flow of the CF-containing intraliposomal solutions. The liposomes should also experience stresses by ice crystal size growth (Ostwald ripening) and rapid dilution of the surrounding media during the thawing process of the frozen suspensions.[23,43]

The different stability-determining factors during the freezing process of the marker-loaded liposomes from those of the living cells suggest requirement of different strategies for their stabilization.[44] Trehalose protected the marker-loaded liposomes through two types of osmotic effects that prevent the freeze-induced internal solution loss during freeze–thawing. The addition of trehalose to both sides of the liposome membrane prevented both the freeze-induced dehydration and water-soluble marker loss, particularly in the higher cooling rate. The marker retention was also achieved by extraliposomal trehalose that osmotically dehydrates the liposomes through outbound water diffusion without apparent CF release in the initial suspensions. The prior dehydration should prevent the freeze-induced membrane damage even in the slower cooling. These osmotic effects should contribute as one of the major mechanisms by which trehalose protects liposomes during the freezing process besides the water-substitution, bulking, and molecular mobility reduction. The liposomes containing sufficiently high concentrations of cryoprotectants can be vitrified without the apparent ice formation by ultrafast cooling (e.g., immersion of small volume suspensions in liquid nitrogen). The vitrification method would not be practical for large-scale freezing of liposome formulations, although it is a popular way to avoid intracellular freezing during cryopreservation of living cells.[12] Formulation and process optimization of liposome pharmaceuticals should be performed through multiple assay methods (e.g., API retention, liposome fusion, aggregation, and activity of encapsulated enzyme) that appropriately detect the changes caused by different stresses.

The varied physical states of the intraliposomal solutions in the frozen suspensions should directly (e.g., membrane damage due to ice growth) or indirectly (e.g., altered excipient–membrane interactions) affect the liposome stability during freeze-drying process and subsequent storage.[1,5,8,45] The trehalose molecules are required to be distributed in the position spatially accessible to the membrane phospholipids to form the water-substituting interactions that protect the membrane structure from the dehydration stresses. The higher glass transition temperatures (T_g) of the dried solids and resistance against changes by absorbed water should make trehalose a potent stabilizer for lyophilization and subsequent storage of liposomes and biomacromolecules.[39] How the altered freezing behavior affects liposome stability during freeze-drying is an intriguing topic for further study.

The present results indicate the relevance of characterizing the freeze-related physical changes of liposomes for the development of frozen or freeze-dried formulations. The liposome composition and trehalose distribution across the membrane significantly affected the osmotic solution flows that determine the physical states of their intraliposomal solutions and functional stabilities (e.g., CF retention) upon freeze–thawing. Potentially varied molecular interactions between components would also affect liposome stability in the subsequent drying process and in storage. Controlling the osmotically mediated physical changes through formulation design and process optimization would be valuable in the cryopreservation and freeze-drying of liposome pharmaceuticals.

REFERENCES

1. Chen C, Han D, Cai C, Tang X. 2010. An overview of liposome lyophilization and its future potential. J Control Release 142:299–311.
2. Misra A, Jinturkar K, Patel D, Lalani J, Chougule M. 2009. Recent advances in liposomal dry powder formulations: Preparation and evaluation. Expert Opin Drug Deliv 6:71–89.
3. van Winden EC. 2003. Freeze-drying of liposomes: Theory and practice. Methods Enzymol 367:99–110.
4. Wessman P, Edwards K, Mahlin D. 2010. Structural effects caused by spray- and freeze-drying of liposomes and bilayer disks. J Pharm Sci 99:2032–2048.
5. Nakagaki M, Nagase H, Ueda H. 1992. Stabilization of the lamellar structure of phosphatidylcholine by complex formation with trehalose. J Memb Sci 73:173–180.
6. Crowe JH, Crowe LM, Chapman D. 1984. Preservation of membranes in anhydrobiotic organisms: The role of trehalose. Science 223:701–703.
7. Ausborn M, Schreierb H, Brezesinskic G, Fabiand H, Meyere HW, Nuhna P. 1994. The protective effect of free and membrane-bound cryoprotectants during freezing and freeze-drying of liposomes. J Control Release 30:105–116.
8. Crowe JH, Crowe LM, Carpenter JF, Rudolph AS, Wistrom CA, Spargo BJ, Anchordoguy TJ. 1988. Interactions of sugars with membranes. Biochim Biophys Acta 947:367–384.
9. Wolfe J, Bryant G. 1999. Freezing, drying, and/or vitrification of membrane-solute-water systems. Cryobiology 39:103–129.
10. Lovelock JE. 1954. The protective action of neutral solutes against haemolysis by freezing and thawing. Biochem J 56:265–270.
11. Rasmussen DH, Macaulay MN, MacKenzie AP. 1975. Supercooling and nucleation of ice in single cells. Cryobiology 12:328–339.
12. Mazur P. 1984. Freezing of living cells: Mechanisms and implications. Am J Physiol 247:C125–C142.

13. Shirakashi R, Tanasawa I. 1998. Method of designing prefreezing protocol in cryopreservation of biological materials. Ann N Y Acad Sci 858:175–182.
14. Mathias SF, Franks F, Hatley RH. 1985. Preservation of viable cells in the undercooled state. Cryobiology 22:537–546.
15. Siow LF, Rades T, Lim MH. 2007. Characterizing the freezing behavior of liposomes as a tool to understand the cryopreservation procedures. Cryobiology 55:210–221.
16. Siow LF, Rades T, Lim MH. 2008. Cryo-responses of two types of large unilamellar vesicles in the presence of non-permeable or permeable cryoprotecting agents. Cryobiology 57:276–285.
17. Talsma H, Van Steenbergen MJ, Crommelin DJ. 1992. The cryopreservation of liposomes. 2. Effect of particle size on crystallization behavior and marker retention. Cryobiology 29:80–86.
18. Charoenrein S, Reid DS. 1989. The use of DSC to study the kinetics of heterogeneous and homogeneous nucleation of ice in aqueous systems. Thermochim Acta 156:373–381.
19. Seki S, Kleinhans FW, Mazur P. 2009. Intracellular ice formation in yeast cells vs. cooling rate: Predictions from modeling vs. experimental observations by differential scanning calorimetry. Cryobiology 58:157–165.
20. Bronshteyn VL, Steponkus PL. 1993. Calorimetric studies of freeze-induced dehydration of phospholipids. Biophys J 65:1853–1865.
21. Lefevre T, Toscani S, Picquart M, Dugue J. 2002. Crystallization of water in multilamellar vesicles. Eur Biophys J 31:126–135.
22. Siminovitch D, Chapman D. 1971. Liposome bilayer model systems of freezing living cells. FEBS Lett 16:207–212.
23. Talsma H, Steenbergen MJV, Crommelin DJA. 1991. The cryopreservation of liposomes: 3. Almost complete retention of a water-soluble marker in small liposomes in a cryoprotectant containing dispersion after a freezing/thawing cycle. Int J Pharm 77:119–126.
24. Harrigan PR, Madden TD, Cullis PR. 1990. Protection of liposomes during dehydration or freezing. Chem Phys Lipids 52:139–149.
25. Higgins J, Hodges NA, Olliff CJ, Phillips AJ. 1986. Factors influencing cryoprotective activity and drug leakage from liposomes after freezing. J Pharm Pharmacol 38:259–263.
26. Hupfeld S, Moen HH, Ausbacher D, Haas H, Brandl M. 2010. Liposome fractionation and size analysis by asymmetrical flow field-flow fractionation/multi-angle light scattering: Influence of ionic strength and osmotic pressure of the carrier liquid. Chem Phys Lipids 163:141–147.
27. Ohtake S, Schebor C, Palecek SP, de Pablo JJ. 2005. Phase behavior of freeze-dried phospholipid-cholesterol mixtures stabilized with trehalose. Biochim Biophys Acta 1713:57–64.
28. Talsma H, van Steenbergen MJ, Salemink PJ, Crommelin DJ. 1991. The cryopreservation of liposomes. 1. A differential scanning calorimetry study of the thermal behavior of a liposome dispersion containing mannitol during freezing/thawing. Pharm Res 8:1021–1026.
29. MacDonald RC, MacDonald RI, Menco BP, Takeshita K, Subbarao NK, Hu LR. 1991. Small-volume extrusion apparatus for preparation of large, unilamellar vesicles. Biochim Biophys Acta 1061:297–303.
30. Kristiansen J. 1992. Leakage of a trapped fluorescent marker from liposomes: Effects of eutectic crystallization of NaCl and internal freezing. Cryobiology 29:575–584.
31. Bartlett GR. 1959. Phosphorus assay in column chromatography. J Biol Chem 234:466–468.
32. Kaasgaard T, Mouritsen OG, Jørgensen K. 2003. Freeze/thaw effects on lipid-bilayer vesicles investigated by differential scanning calorimetry. Biochim Biophys Acta 1615:77–83.
33. Wu WG, Chi LM, Yang TS, Fang SY. 1991. Freezing of phosphocholine headgroup in fully hydrated sphingomyelin bilayers and its effect on the dynamics of nonfreezable water at subzero temperatures. J Biol Chem 266:13602–13606.
34. Rall WF, Mazur P, McGrath JJ. 1983. Depression of the ice-nucleation temperature of rapidly cooled mouse embryos by glycerol and dimethyl sulfoxide. Biophys J 41:1–12.
35. Nagle JF, Wilkinson DA. 1978. Lecithin bilayers. Density measurement and molecular interactions. Biophys J 23:159–319.
36. Koster KL, Lei YP, Anderson M, Martin S, Bryant G. 2000. Effects of vitrified and nonvitrified sugars on phosphatidylcholine fluid-to-gel phase transitions. Biophys J 78:1932–1946.
37. Mui BL, Cullis PR, Evans EA, Madden TD. 1993. Osmotic properties of large unilamellar vesicles prepared by extrusion. Biophys J 64:443–453.
38. Akers MJ, Vasudevan V, Stickelmeyer M. 2002. Formulation development of protein dosage forms. Pharm Biotechnol 14:47–127.
39. Nail SL, Jiang S, Chongprasert S, Knopp SA. 2002. Fundamentals of freeze-drying. Pharm Biotechnol 14:281–360.
40. Blok MC, van Deenen LL, De Gier J. 1976. Effect of the gel to liquid crystalline phase transition on the osmotic behaviour of phosphatidylcholine liposomes. Biochim Biophys Acta 433:1–12.
41. Pencer J, White GF, Hallett FR. 2001. Osmotically induced shape changes of large unilamellar vesicles measured by dynamic light scattering. Biophys J 81:2716–2728.
42. Suzuki T, Komatsu H, Miyajima K. 1996. Effects of glucose and its oligomers on the stability of freeze-dried liposomes. Biochim Biophys Acta 1278:176–182.
43. Grabielle-Madelmont C, Perron R. 1983. Calorimetric studies on phospholipid-water systems: II. Study of water behavior. J Colloid Interface Sci 95:483–493.
44. Hubel A, Darr TB, Chang A, Dantzig J. 2007. Cell partitioning during the directional solidification of trehalose solutions. Cryobiology 55:182–188.
45. Ohtake S, Schebor C, de Pablo JJ. 2006. Effects of trehalose on the phase behavior of DPPC-cholesterol unilamellar vesicles. Biochim Biophys Acta 1758:65–73.

International Journal of Pharmaceutics 407 (2011) 111–118

Contents lists available at ScienceDirect

International Journal of Pharmaceutics

journal homepage: www.elsevier.com/locate/ijpharm

Differences in crystallization rate of nitrendipine enantiomers in amorphous solid dispersions with HPMC and HPMCP

Tamaki Miyazaki[a,*], Yukio Aso[a], Sumie Yoshioka[b], Toru Kawanishi[a]

[a] Division of Drugs, National Institute of Health Sciences, 1-18-1 Kamiyoga, Setagaya-ku, Tokyo 158-8501, Japan
[b] School of Pharmacy, University of Connecticut, Storrs, CT, United States

ARTICLE INFO

Article history:
Received 21 October 2010
Received in revised form
21 December 2010
Accepted 19 January 2011
Available online 26 January 2011

Keywords:
Nitrendipine
Enantiomer
Chiral polymer
Solid dispersions
Crystallization

ABSTRACT

To clarify the contribution of drug–polymer interaction to the physical stability of amorphous solid dispersions, we studied the crystallization rates of nitrendipine (NTR) enantiomers with identical physicochemical properties in the presence of hydroxypropylmethylcellulose (HPMC), hydroxypropylmethylcellulose phthalate (HPMCP) and polyvinylpyrrolidone (PVP). The overall crystallization rate at 60 °C and the nucleation rate at 50–70 °C of (+)-NTR were lower than those of (−)-NTR in the presence of 10–20% HPMC or HPMCP. In contrast, similar crystallization profiles were observed for the NTR enantiomers in solid dispersions containing PVP. The similar glass transition temperatures for solid dispersions of (−)-NTR and (+)-NTR suggested that the molecular mobility of the amorphous matrix did not differ between the enantiomers. These results indicate that the interaction between the NTR enantiomers and HPMC or HPMCP is stereoselective, and that differences in the stereoselective interaction create differences in physical stability between (−)-NTR and (+)-NTR at 50–70 °C. However, no difference in physical stability between the enantiomers was obvious at 40 °C. Loss of the difference in physical stability between the NTR enantiomers suggests that the stereoselective interaction between NTR and the polymers may not contribute significantly to the physical stabilization of amorphous NTR at 40 °C.

1. Introduction

Nifedipine analogues are used for treatment of cardiovascular disorders. Most of them are poorly water soluble and their bioavailability is low when administered orally in crystal form. To improve the bioavailability by increasing the dissolution rate and solubility, amorphous solid dispersions of nifedipine analogues have been studied over the past few decades (Suzuki and Sunada, 1998; Chutimaworapan et al., 2000; Vippagunta et al., 2002; Hirasawa et al., 2003a,b, 2004; Tanno et al., 2004; Karavas et al., 2005, 2006; Wang et al., 2005, 2007; Kim et al., 2006; Konno and Taylor, 2006; Huang et al., 2008; Marsac et al., 2008; Rumondor et al., 2009a,b). Drugs in an amorphous state are more easily dissolved in water than their crystalline counterparts. However, recrystallization to a thermodynamically stable form during long-term storage is a matter of concern. The physical stability of amorphous solid dispersions (crystallization tendency) has been reported to correlate with several factors, such as molecular mobility (Aso et al., 2004; Miyazaki et al., 2007), drug–excipient interactions and miscibility (Matsumoto and Zografi, 1999; Marsac et al., 2006, 2009; Miyazaki et al., 2004, 2006, 2007; Konno and Taylor, 2006; Haddadin et al., 2009; Tao et al., 2009; Telang et al., 2009). The crystallization rate of amorphous nitrendipine (NTR) increases with a decrease in the glass transition temperature (T_g) associated with water sorption, indicating that molecular mobility, in terms of T_g, is correlated with physical stability. However, amorphous nilvadipine is more stable than nifedipine, even though the two had similar T_g values, indicating that the difference in physical stability between nilvadipine and nifedipine might be attributable to differences in chemical structure (Miyazaki et al., 2007). Hydrogen bond interaction between felodipine and hydroxypropylmethylcellulose (HPMC) or hydroxypropylmethylcellulose acetate succinate is considered to decrease the nucleation rate of felodipine, since no significant change in molecular mobility, reflected in T_g value, has been observed (Konno and Taylor, 2006). Also, drug–excipient miscibility is reportedly related to the physical stability of nifedipines. Drug crystallization has been observed to occur earlier in solid dispersions showing phase separation due to low miscibility of the drug with the excipient polymers (Rumondor et al., 2009a,b; Marsac et al., 2010). In order to develop stable amorphous solid dispersions, it is important to clarify the relative significance of these factors for the physical stability of amorphous solid dispersions. Therefore, designing a model system that is as simple as possible is the key to evaluation of each individual factor.

NTR has an asymmetric carbon (Fig. 1), and is available as a mixture of both enantiomers. These enantiomers can be resolved by chiral chromatography. Since both enantiomers have identical physical and chemical properties, including molecular mass, T_g,

* Corresponding author. Tel.: +81 3 3700 1141; fax: +81 3 3707 6950.
E-mail address: miyazaki@nihs.go.jp (T. Miyazaki).

0378-5173/$ – see front matter © 2011 Elsevier B.V. All rights reserved.
doi:10.1016/j.ijpharm.2011.01.035

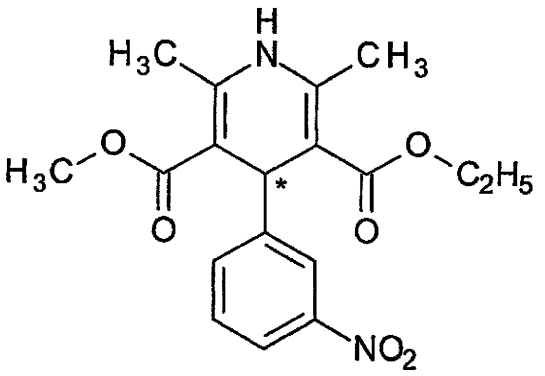

Fig. 1. Chemical structure of NTR. The asterisk represents asymmetric carbon.

melting point and density, the effects of molecular mobility and chemical structure on their physical stability are expected to be the same. Therefore, solid dispersions of NTR enantiomers may provide a useful model system for studies of drug–polymer stereoselective interaction. In the present study, HPMC and hydroxypropylmethylcellulose phthalate (HPMCP) were used as chiral polymers, and polyvinylpyrrolidone (PVP), an achiral polymer, was selected as a control to investigate the effect of drug–polymer interaction on the physical stability of amorphous NTR enantiomers. The overall crystallization rates were determined from the time-profiles of amorphous drug remaining, as measured by differential scanning calorimetry (DSC). Furthermore, the nucleation and the crystal growth rates of each NTR enantiomer in the solid dispersions containing HPMC, HPMCP or PVP were determined by polarized light microscopy. Measurements of T_g and Fourier-transform infrared spectra (FT-IR) were carried out for evaluation of molecular mobility and drug–polymer interactions, respectively.

2. Materials and methods

2.1. Materials

PVP (PVP10) and HPMC (USP grade) were purchased from Sigma–Aldrich, Inc. HPMCP (HP-55) was kindly obtained from Shin-Etsu Chemical Co., Ltd.

NTR (Wako Pure Chemical Industries Ltd.) was resolved on a CHIRALCEL OJ-H column (Daicel Chemical Industries, Ltd., 10 mm × 250 mm) into two fractions of each enantiomer with a mobile phase of n-hexane/ethanol (100/15, flow rate: 4 ml/min). A 500 μl of 1% NTR solution in n-hexane/ethanol (1/1) was injected, and ultraviolet spectrophotometric detection was carried out at 254 nm. The circular dichroism spectrum of the first fraction exhibited a negative peak at around 360 nm, and the second one exhibited a positive peak. Therefore, the first and second fractions of NTR were designated (−)-NTR and (+)-NTR, respectively. The optical purity of each enantiomer was determined to be more than 99.96%, and the amount of photo degradation product of NTR was determined to be less than 0.03% by liquid chromatography, on a CHIRALCEL OJ-H column (Daicel Chemical Industries, Ltd.,

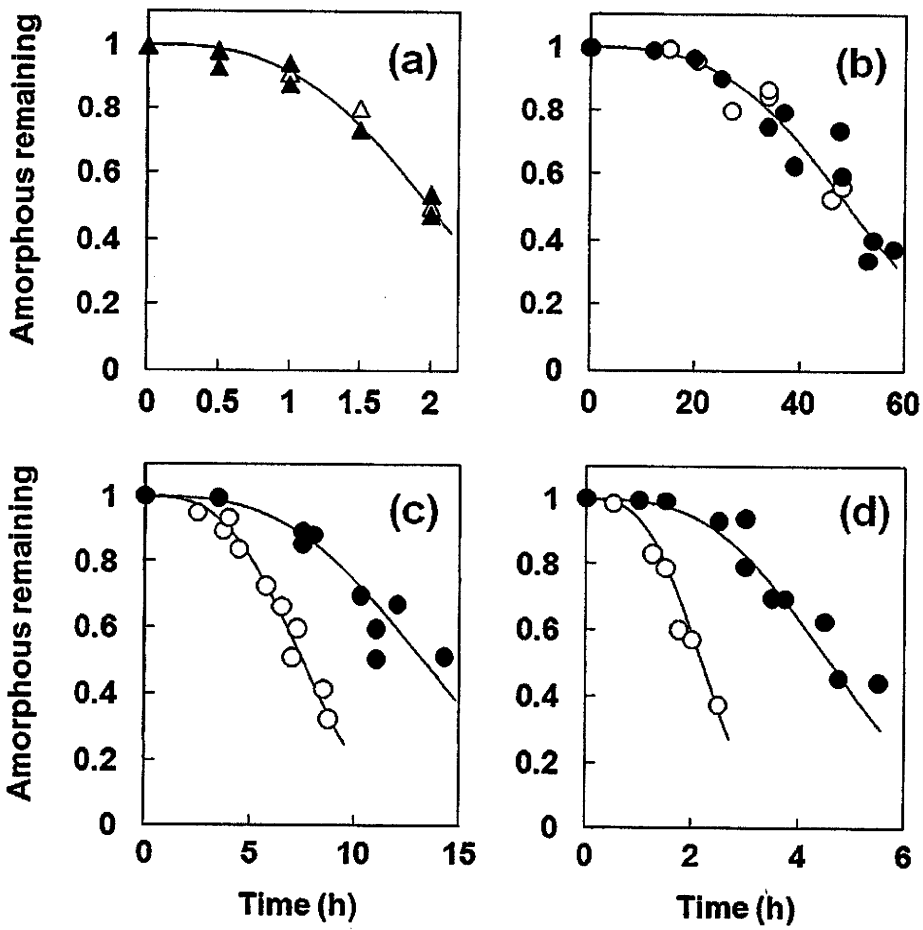

Fig. 2. Crystallization profiles of each NTR enantiomer alone ((a); △, ▲) and the enantiomers in solid dispersions (○, ●) with (b) 10% PVP, (c) 10% HPMC and (d) 10% HPMCP at 60 °C. Open symbols represent (−)-NTR and solid symbols represent (+)-NTR. The lines in the figures represent the best fit of the Avrami equation.

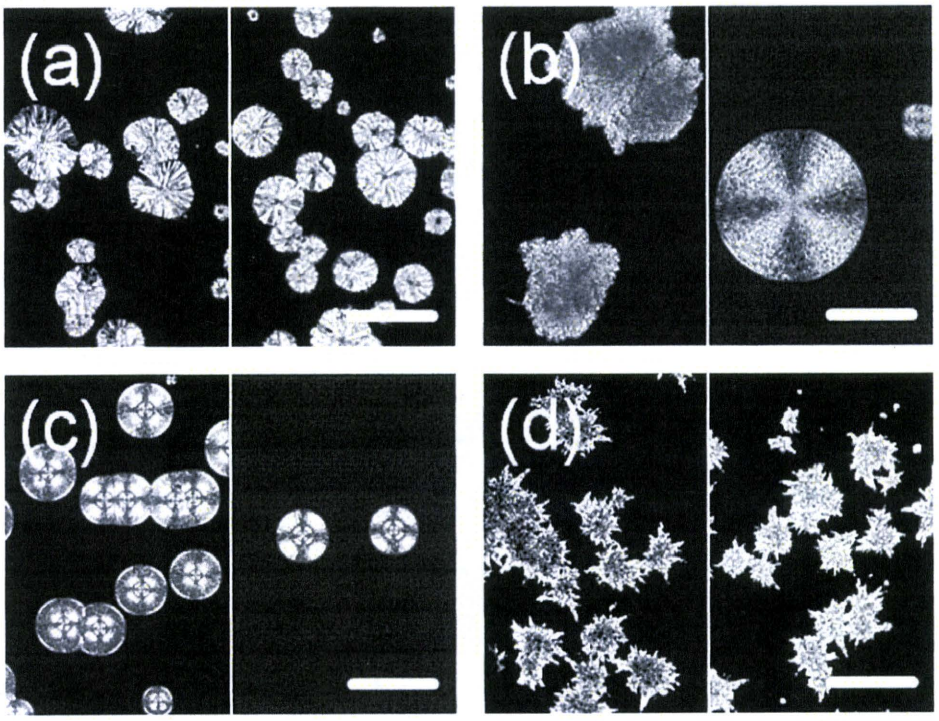

Fig. 3. Typical crystal shape observed for the amorphous NTR enantiomers and their solid dispersions: (a) without polymer, (b) 10% HPMC, (c) 10% HPMCP and (d) 10% PVP. The left side of each micrograph was taken from the (−)-NTR samples, and the right side from the (+)-NTR samples. The bars in the micrographs correspond to 100 μm.

4.6 mm × 250 mm) with a mobile phase of n-hexane/ethanol = 10/1 (1 ml/min). Since NTR is a photo sensitive compound, NTR samples were handled under dim light (<120 lx).

2.2. Determination of the overall crystallization rate of amorphous NTR enantiomers

Amorphous solid dispersions of the NTR enantiomers were prepared by melt-quenching drug–polymer mixtures. One NTR enantiomer and a polymer were initially dissolved in a solvent that was suitable for both components. Ethanol/acetone (1:1) was used for the NTR–HPMC and NTR–HPMCP combinations, and ethanol was used for the NTR–PVP combination. Next, the solvent was rotary-evaporated to obtain a homogeneous drug–polymer mixture. Approximately 4 mg of the pulverized mixture was weighed into an aluminum pan for DSC, and was kept at around 180 °C in the cell of a DSC (DSC2920, TA Instruments) for approximately 2 min under dry nitrogen gas flow (30 ml/min). The melted sample was transferred to a desiccator containing phosphorus pentoxide, and the desiccator was stored at a constant temperature of 30–70 °C. For the pure NTR enantiomer, the resolved enantiomer crystal (4 mg) was melt-quenched as described above to obtain an amorphous sample.

After certain periods of time, the change in heat capacity (ΔC_p) at T_g was measured for the stored amorphous samples by DSC at a heating rate of 20 °C/min. The amount of amorphous drug remaining in the sample at time t, $x(t)$, was calculated according to Eq. (1):

$$x(t) = \frac{\Delta C_{pt}}{\Delta C_{p0}} \quad (1)$$

where ΔC_{pt} and ΔC_{p0} are the ΔC_p values at time t and initially, respectively. The time required for 10% of the amorphous NTR to crystallize (t_{90}) was estimated as an indicator of the crystallization tendency. The time-profiles of $x(t)$ were analyzed according to the Avrami equation (Eq. (2), $n = 3$) to calculate t_{90}:

$$x(t) = \exp[-kt^n] \quad (2)$$

where k is the crystallization rate constant and n is the Avrami index. HPLC analysis of stored NTR samples showed no evidence of degradation during melt-quenching and subsequent storage.

2.3. Determination of nucleation rate and crystal growth rate of NTR enantiomer

The nucleation rate and the crystal growth rate were determined for samples prepared in a space between two glass disks separated by a stainless steel ring. The NTR enantiomer–polymer mixture, which was described above, or the crystalline NTR enantiomer (1.5–2 mg) was placed on a clean glass disk (thickness: 0.12 mm, diameter: 16 mm) and heated at 180 °C in the DSC with a stainless steel ring (inner diameter: 6 mm, thickness: 20 μm) as a spacer. After the sample had melted completely, it was covered with another glass disk (thickness: 0.12 mm, diameter: 12 mm) to yield an amorphous layer between the glasses. Attention was paid to ensure that the layer was free of bubbles. For measurements at temperatures above 40 °C, the sample was stored in the chamber of a heating/cooling stage for microscopy (THMS600, Linkam Scientific Instruments), which had been adjusted to a prescribed temperature in advance. The moisture in the chamber was removed by purging with dry nitrogen gas for 10–15 min. Microscopic images of the sample were recorded at appropriate time intervals by a digital camera (DXM1200F, Nikon Corporation) attached to a polarized light microscope (ECLIPSE E600 POL, Nikon Corporation) with a 10× objective lens. In order to minimize possible photo degradation of NTR by the polarized light, the light source of the microscope was shut off when images were not recorded. For measurements at 30 °C, the samples were stored at 30 °C in desiccators containing phosphorous pentoxide. After an appropriate period of storage, microscopic images of the sample were recorded, and the sample was again stored at 30 °C in a dry state.

2.3.1. Measurement of nucleation rate

The nucleation rate of the NTR enantiomers was estimated from time-profiles of nucleation site density determined from microscopic images of the stored samples. Nucleation site density per unit volume was calculated from the number of nucleation sites per unit area and the depth of field of the lens used for data collection. The depth of field was calculated to be 8.46 μm from the wavelength of the light (546 nm) and the numerical aperture of the lens (0.25). For samples with more than a dozen nucleation sites per fixed field at the end of the observation period, nucleation sites were counted in one fixed field. For samples with less than a dozen nucleation sites per field near the end of the observation period, and those stored at 30 °C, nucleation sites were counted for 12 individual areas in one sample, and the average value from the 12 individual images was regarded as the number of nucleation sites per field. The nucleation rate was obtained from the slope of time-profiles of the number of nucleation sites per unit volume (nucleation site density) at steady state. In cases showing preferential nucleation and growth at the sample periphery, these sites were not included in the analysis. The reported nucleation rates were average values of those obtained for at least three samples prepared separately.

2.3.2. Measurement of crystal growth rate

The crystal growth rates at temperatures above 40 °C were measured concurrently with the nucleation rate measurements as described above. The measurements at 30 °C were carried out using samples that showed more than a dozen nucleation sites per one field after a few months of storage in desiccators containing phosphorous pentoxide. The sample was placed in the chamber of the heating/cooling stage controlled at 30 °C, and the growth of crystals was observed in a fixed field. The radius of each crystal was estimated from a circular approximation by using Lumina Vision software (Mitani Co.). The average crystal growth rate was calculated from the increase in the radius as a function of time based on observations of at least 20 crystals.

2.4. FT-IR

FI-IR spectra were collected using a FT/IR-6300 (JASCO Corporation) by the KBr method at ambient room temperature. Transmission spectra were obtained for KBr disks containing 1–1.5% sample at a resolution of 0.4 cm^{-1} within the range of 4000–400 cm^{-1}. An accumulation of 128–256 scans was acquired for each disk.

3. Results

3.1. Effects of polymers on the overall crystallization rates of NTR enantiomers in solid dispersions

No significant differences in the melting point (158 °C), T_g (33 °C) and ΔC_p at T_g (0.40 J/g/K) were observed between (−)-NTR and (+)-NTR. Table 1 shows the T_g values of amorphous solid dispersions of (−)-NTR and (+)-NTR. There appeared to be no significant difference in the T_g values between the two. The solid dispersions containing HPMC (10–20%) and 5% PVP showed T_g values similar to that of each NTR enantiomer alone. T_g values for solid dispersions containing 10% PVP were slightly higher than that of each NTR enantiomer alone, whereas solid dispersions containing HPMCP (10–20%) exhibited T_g values slightly lower than that of each NTR enantiomer alone.

Fig. 2 shows time-profiles of overall crystallization of NTR enantiomers at 60 °C. No significant differences in the overall crystallization profiles were observed between (−)-NTR and (+)-NTR without polymer (Fig. 2(a)), and between (−)-NTR and (+)-NTR in solid dispersions containing 10% PVP (Fig. 2(b)). In contrast, differences in time-profiles between the enantiomers were observed for solid dispersions containing 10% HPMC or HPMCP: (+)-NTR crystallized more slowly than (−)-NTR, as shown in Fig. 2(c) and (d). Table 2 shows the t_{90} values for the amorphous NTR enantiomers obtained for NTR alone and NTR in the solid dispersions. The t_{90} values for (−)-NTR without polymer and those of solid dispersions containing 5–10% PVP were almost the same as the t_{90} values for (+)-NTR without polymer and those of solid dispersions containing 5–10% PVP, respectively, at the temperatures studied. The t_{90} values at 50 and 60 °C for (+)-NTR were 1.5–2.0 times longer than that for (−)-NTR in solid dispersions containing 10–20% HPMC or HPMCP. At 40 °C, however, any difference between the enantiomers was not clear.

Table 1
T_g of pure NTR enantiomers and their solid dispersions with a polymer.

Polymer	Polymer content [%]	T_g[a] [°C]	
		(−)-NTR	(+)-NTR
None	0	33.2 ± 0.1	33.1 ± 0.2
HPMC	10	33.1 ± 1.0	33.0 ± 0.7
	20	33.1 ± 0.8	33.0 ± 0.7
HPMCP	10	31.2 ± 0.7	31.0 ± 0.4
	20	30.8 ± 1.2	30.5 ± 0.9
PVP	5	33.0 ± 0.2	33.1 ± 0.2
	10	36.3 ± 1.2	36.2 ± 0.8

[a] Average ± standard deviation (n = 3).

3.2. Effects of polymers on the nucleation rate and crystal growth rate

Fig. 3 shows the typical micrographs of NTR crystals grown from amorphous pure enantiomers and their solid dispersions with a polymer. The recrystallized NTR enantiomers without polymers showed a melting point of 158 °C, suggesting the same crystal form as the originally resolved stable one. The melting point of the samples containing 10% HPMC, HPMCP and PVP was approximately 151 °C in all cases, regardless of the various crystal shapes shown in Fig. 3. The difference from the melting point of the pure enantiomers would have been due to melting point depression by the

Table 2
t_{90} for NTR enantiomers with and without polymer.

Temperature [°C]	Polymer	[%]	t_{90}[a] [h]			
			(−)-NTR		(+)-NTR	
40	None	0	41	(1)	41	(1)
	HPMC	10	230, 240[b]		230, 230[b]	
	HPMCP	10	49	(1)	49	(1)
50	None	0	5.7	(0.2)	5.7	(0.1)
	PVP	10	250	(10)	240	(4)
	HPMC	10	17	(0.4)	25	(0.1)
	HPMCP	10	6.1	(0.3)	11	(0.3)
60	None	0	1.1	(0.1)	1.1	(0.1)
	PVP	5	3.5	(0.1)	3.6	(0.1)
		10	25 ± 3[c]		25 ± 3[c]	
	HPMC	10	3.8, 4.1[b]		6.7, 6.9[b]	
		20	8.7	(0.3)	15	(0.4)
	HPMCP	10	1.5 ± 0.2[c]		2.7 ± 0.3[c]	
		20	3.2	(0.1)	6.4	(0.2)

[a] The values in parentheses are standard error estimated from single experiments using Origin 8.1 software (Lightstone Corp.).
[b] Results with two values represent the results obtained from duplicate experiments using separately prepared samples.
[c] Mean ± standard deviation (n = 3).

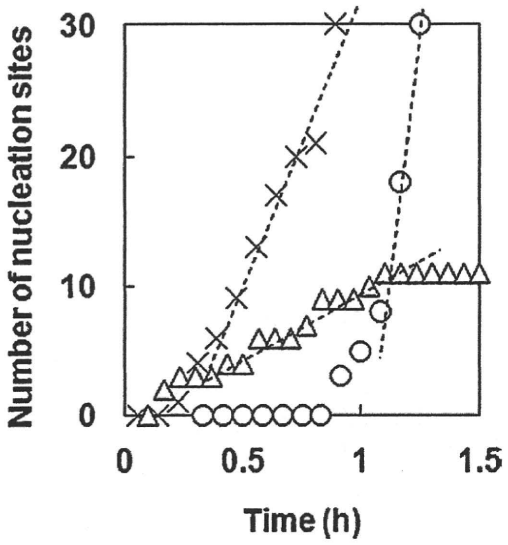

Fig. 4. Time profiles of the number of nucleation sites per field of view for (+)-NTR at 50 °C (○), 60 °C (×) and 70 °C (△). The dotted lines show the linear regression at steady state.

added polymers, as the melting point fell gradually with increasing polymer content (data not shown). The data suggested that differences in crystal habit, rather than polymorphism, might have been responsible for the differences in crystal shape among the solid dispersions.

Fig. 4 shows the typical time-profiles of the nucleation of amorphous NTR enantiomer stored at various temperatures. The lower the storage temperature, the longer the period required before the first crystal was observed. The nucleation rates at steady state were obtained from the slope of the lines in Fig. 4, and these were plotted against storage temperature (Fig. 5). As expected from the similar overall crystallization profiles of the NTR enantiomers (Fig. 2(a) and (b)), no significant difference in the nucleation rates between (−)-NTR and (+)-NTR was observed for amorphous NTR alone and the solid dispersions containing PVP within the temperature range studied (Fig. 5(a)). In contrast, the nucleation rates of (+)-NTR were lower than those of (−)-NTR in the solid dispersions containing HPMC and HPMCP (Fig. 5(b)) within the temperature range of 50–70 °C. At 40 °C, however, the differences in the rates between (−)-NTR and (+)-NTR were not pronounced. These results were consistent with the t_{90} values of the enantiomers shown in Table 2.

Fig. 6 shows the typical time-profiles of the NTR crystal growth at 60 °C. Crystal radius increased linearly with time, and the growth rate was estimated from linear regression of the plots. The higher the temperature, the faster the crystals grew within the temperature range studied (Fig. 7). In contrast to the nucleation rates, no significant growth rate differences between the NTR enantiomers were observed, irrespective of the absence or presence of any polymer.

3.3. FT-IR

FT-IR spectra (4000–400 cm^{-1}) of (−)-NTR and (+)-NTR were indistinguishable from one another for both the amorphous and the crystalline forms. Similarly, the FT-IR spectra of amorphous solid dispersions were almost the same for (−)-NTR and (+)-NTR with any polymer. Fig. 8 shows the spectra for crystalline (−)-NTR (dotted line in Fig. 8 (a)), NTR solid dispersions containing 25–75% HPMC and HPMC alone (dotted line in Fig. 8 (c)) in the range of 1800–1550 cm^{-1}, corresponding to C=O stretching region of NTR. Spectra with and without an asterisk represent that of (−)-NTR

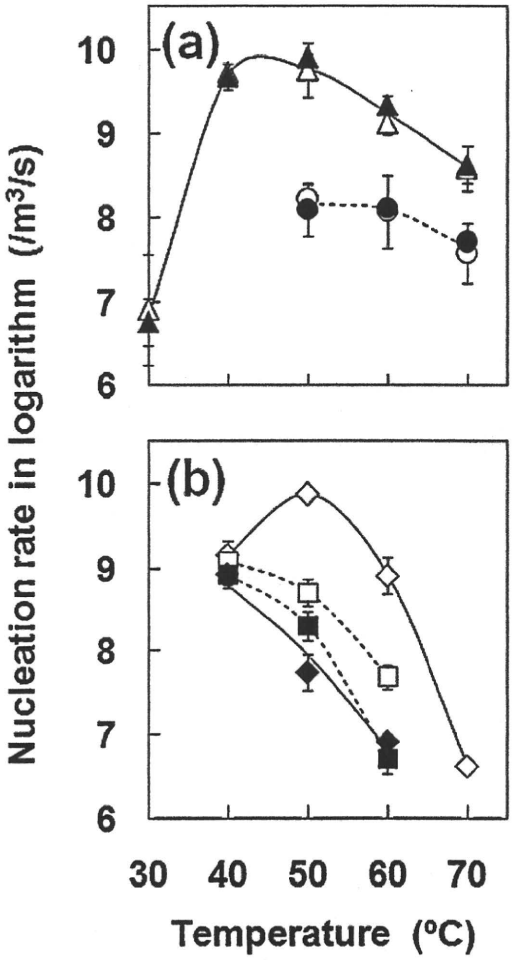

Fig. 5. Plots of nucleation rate as a function of temperature. Error bars represent standard deviation for at least triplicate experiments. (a) △, ▲: without polymer, ○, ●: 10% PVP and (b) □, ■: 10% HPMC, ◊, ♦: 10% HPMCP. Open symbols represent (−)-NTR and solid symbols represent (+)-NTR.

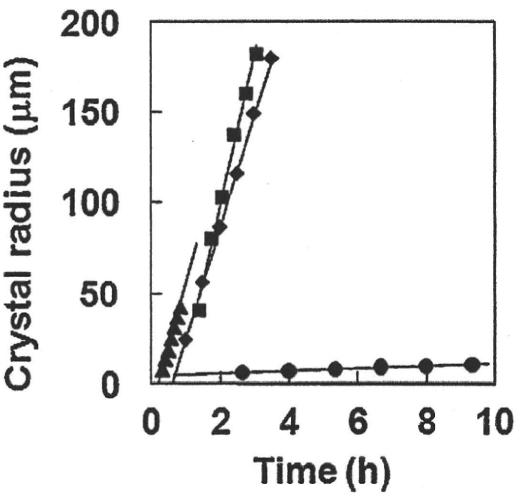

Fig. 6. Typical time profiles of the radius of NTR crystals in (+)-NTR alone (▲), and solid dispersions with 10% HPMC (■), 10% HPMCP (♦) and 10% PVP (●) at 60 °C.

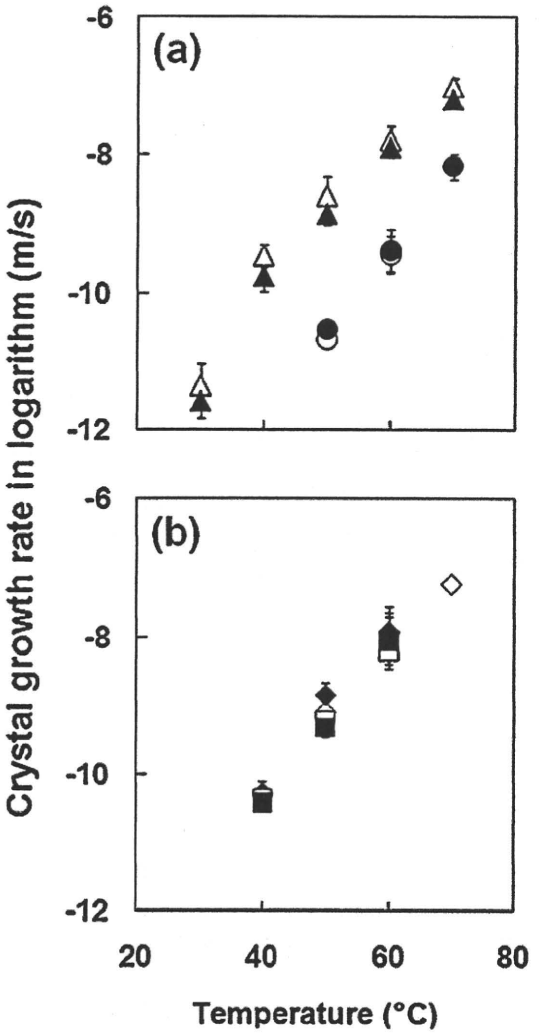

Fig. 7. Temperature dependence of crystal growth rate of NTR enantiomers. Error bars represent standard deviation for at least triplicate experiments. (a) △, ▲: without polymer; ○, ●: 10% PVP and (b) □, ■: 10% HPMC; ◇, ◆: 10% HPMCP. Open symbols represent (−)-NTR and solid symbols represent (+)-NTR.

and (+)-NTR, respectively. Despite its vicinity to the asymmetric carbon, carbonyl group of (−)-NTR and (+)-NTR showed same spectra even in the presence of HPMC. Likewise, no difference in spectra between solid dispersions of (−)-NTR and (+)-NTR containing HPMCP was observed (data not shown).

Fig. 9 shows the spectra in the range of 3650–3150 cm^{-1}, corresponding to NH stretching vibrations of nifedipine derivatives (Konno and Taylor, 2006), where the changes in peak position were obvious upon mixing with polymers as solid dispersions. There were also no obvious differences in the spectra between the two enantiomers. The peak around 3350 cm^{-1} was assigned to the NH stretching vibration that was expected to be involved in the hydrogen bonding between the drug and a polymer. The peak position was shifted from 3360 cm^{-1} to 3337 cm^{-1} by amorphization, and additionally shifted to 3291 cm^{-1} in the presence of 50% PVP (Figs. 9(b) and 10). On the other hand, for solid dispersions prepared with HPMC and HPMCP, the peak position showed a degree of shift to a higher wavenumber (Figs. 9(c) and (d) and 10). The peak position for solid dispersions with 75% HPMCP was nearly equal to that of the pure NTR crystals. These changes in peak position showed the same tendency for both (+)-NTR and (−)-NTR.

4. Discussion

The overall crystallization of (−)-NTR proceeded faster than that of (+)-NTR in solid dispersions with HPMC or HPMCP (Fig. 2(c) and (d)), while that for solid dispersions with PVP proceeded at almost the same rate, regardless of NTR chirality (Fig. 2(b)). The nucleation rates of (−)-NTR were greater than those of (+)-NTR in solid dispersions with HPMC or HPMCP at 50–70 °C (Fig. 5(b)), while no difference in nucleation rates between the NTR enantiomers was observed for solid dispersions with PVP (Fig. 5(a)). The T_g values for samples using (−)-NTR or (+)-NTR were almost the same (Table 1), suggesting that the differences in the overall crystallization profiles and nucleation rates between the enantiomers are not due to differences in molecular mobility between (−)-NTR and (+)-NTR in solid dispersions with HPMC or HPMCP. The difference in physical stability between the two enantiomers may be explained by the difference in strength of NTR–polymer interaction between them. The results obtained from FT-IR measurements indicate that PVP interacts with NTR through hydrogen bonding at the NH moiety of NTR (Figs. 9 and 10). Almost the same degrees of shift in wavenumber for NH stretching suggest a similar strength of hydrogen bond interaction for (−)-NTR and (+)-NTR. PVP polymer chains possess an asymmetric carbon in a monomer unit, and are composed of monomer units with an equal ratio of R and S configurations. Therefore, (−)-NTR and (+)-NTR are considered to interact with PVP through hydrogen bonds of the same strength and number, resulting in a similar degree of physical stability between (−)-NTR and (+)-NTR. In contrast, HPMC and HPMCP are cellulose derivatives that are polymers of optically active D-glucose, and thus are expected to interact differently (strength and/or number) with NTR enantiomers, resulting in the difference in physical stability between (−)-NTR and (+)-NTR, although differences in interaction were not detectable by FT-IR. At 40 °C, however, the differences in physical stability between the enantiomers with HPMC or HPMCP were not remarkable (Table 2, Fig. 5). We do not have a satisfactory explanation for the loss of the difference in stabilization by HPMC and HPMCP. However, one possible explanation is as follows: The temperature dependence of the nucleation rate exhibits a maximum just above T_g because the nucleation rate is influenced by both molecular mobility and thermodynamic factors; an increase of temperature increases the molecular mobility, and thus the nucleation rate, whereas nucleation is thermodynamically favored at lower temperatures. A barrier due to molecular mobility is considered to play a predominant role in nucleation within the temperature range below the maximum point (Hancock and Zografi, 1997; Andronis and Zografi, 2000). Therefore, loss of the difference in physical stability between the enantiomers at 40 °C may be due to the predominant contribution of molecular mobility, since the molecular mobility is suggested to be similar for (−)-NTR and (+)-NTR in solid dispersions, as indicated by the T_g values (Table 1). However, physical stability data at temperatures below 40 °C, which are difficult to obtain within the commonly used experimental time scale, are needed in order to support this speculation.

In contrast to the nucleation rates, no significant difference in the crystal growth rates between the NTR enantiomers was observed for solid dispersions with HPMC or HPMCP (Fig. 7). The crystal growth rates for solid dispersions with HPMC or HPMCP were similar to those for each NTR enantiomer alone, indicating that the effects of HPMC and HPMCP on the crystal growth rate were small. This might be one of the reasons why differences in the crystal growth rate between the NTR enantiomers could not be detected in solid dispersions with HPMC or HPMCP.

It may be worth to note that PVP decreased the crystal growth rate of NTR enantiomers more than HPMC and HPMCP at all the temperatures studied (Fig. 7). On the other hand, PVP did not always decrease the nucleation rate of NTR more effectively than HPMC or

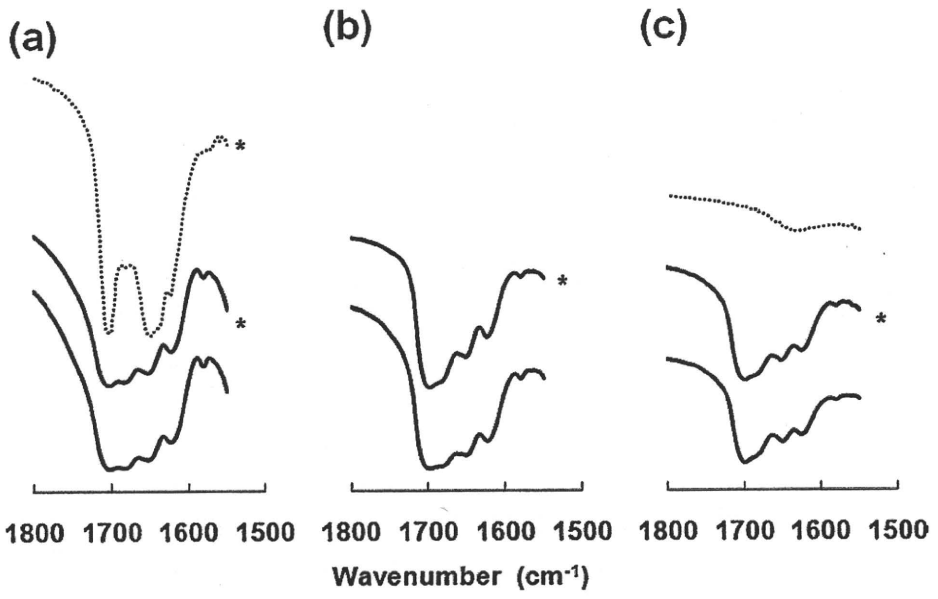

Fig. 8. FT-IR spectra of crystalline (−)-NTR, solid dispersions of NTR enantiomer containing HPMC, and HPMC alone. HPMC content was (a) 25% (b) 50%, and (c)75%. Dotted line in (a) represents the spectrum for crystalline (−)-NTR, and dotted line in (c) represents the spectrum for HPMC alone. The spectra with an asterisk are those of (−)-NTR.

HPMCP. For example, the nucleation rate of NTR at 60°C was following order; (−)-NTR, (+)-NTR ≈ (−)-NTR–HPMCP > (−)-NTR–PVP, (+)-NTR–PVP > (−)-NTR–HPMC > (+)-NTR–HPMC, (+)-NTR–HPMCP (Fig. 5). PVP seems to decrease the crystal growth rate more effectively than the nucleation rate of NTR, whereas HPMC and HPMCP decrease only the nucleation rate of NTR. The reason for the different stabilizing effects of the polymers for the nucleation and crystal growth of NTR is not clear. The growth rate of NTR may only be decreased by strong interactions such as hydrogen bonding between NTR and PVP, which is detectable by FT-IR (Figs. 9 and 10). Weak drug–polymer interactions, which are not detectable by FT-IR, may decrease the nucleation rate of NTR, as well as hydrogen bond interactions between drug and polymer.

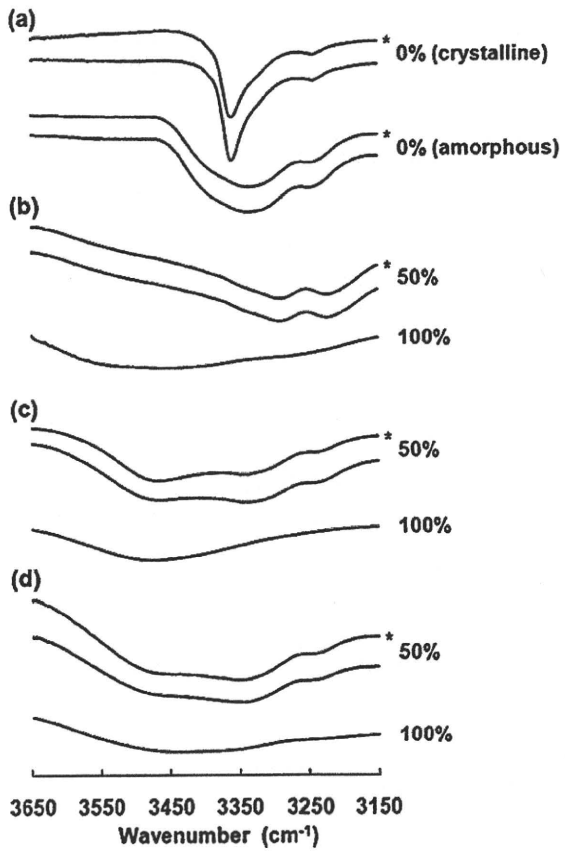

Fig. 9. FT-IR spectra of (a) crystalline and amorphous NTR enantiomers, and their amorphous solid dispersions with (b) PVP, (c) HPMC and (d) HPMCP. Percentages represent the weight percentage of polymer in the solid dispersions. The spectra with an asterisk are those of (−)-NTR.

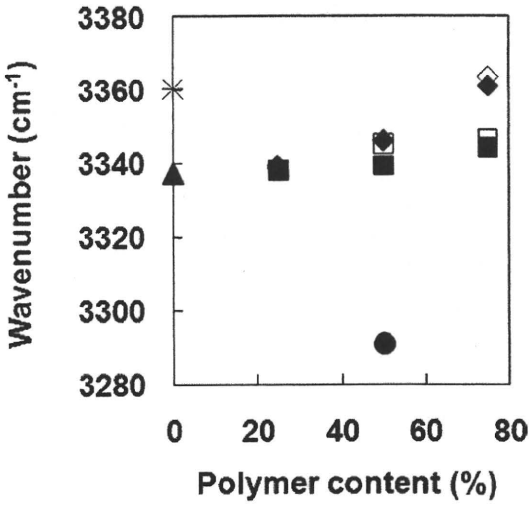

Fig. 10. Changes in FT-IR peak position showing the NH stretching region. +: (−)-NTR without polymer (crystalline); ×: (+)-NTR without polymer (crystalline); △, ▲: without polymer (amorphous); □, ■: HPMC; ◇, ◆: HPMCP; ○, ●: PVP. Open symbols represent (−)-NTR and solid symbols represent (+)-NTR.

5. Conclusions

Using NTR enantiomers as model drugs, the effects of stereoselective drug–polymer interaction on the crystallization rate of amorphous solid dispersions were elucidated. The chiral polymers, HPMC and HPMCP, retarded the crystallization of (+)-NTR more